North Pacific Observation System of Space Weather

Institute of Cosmophysical Research and Radio Wave Propagation
Far Eastern Branch of Russian Academy of Science ***(IKIR FEB RAS)***

B.M. Shevtsov

Position of Stations
Equipment
Communication system

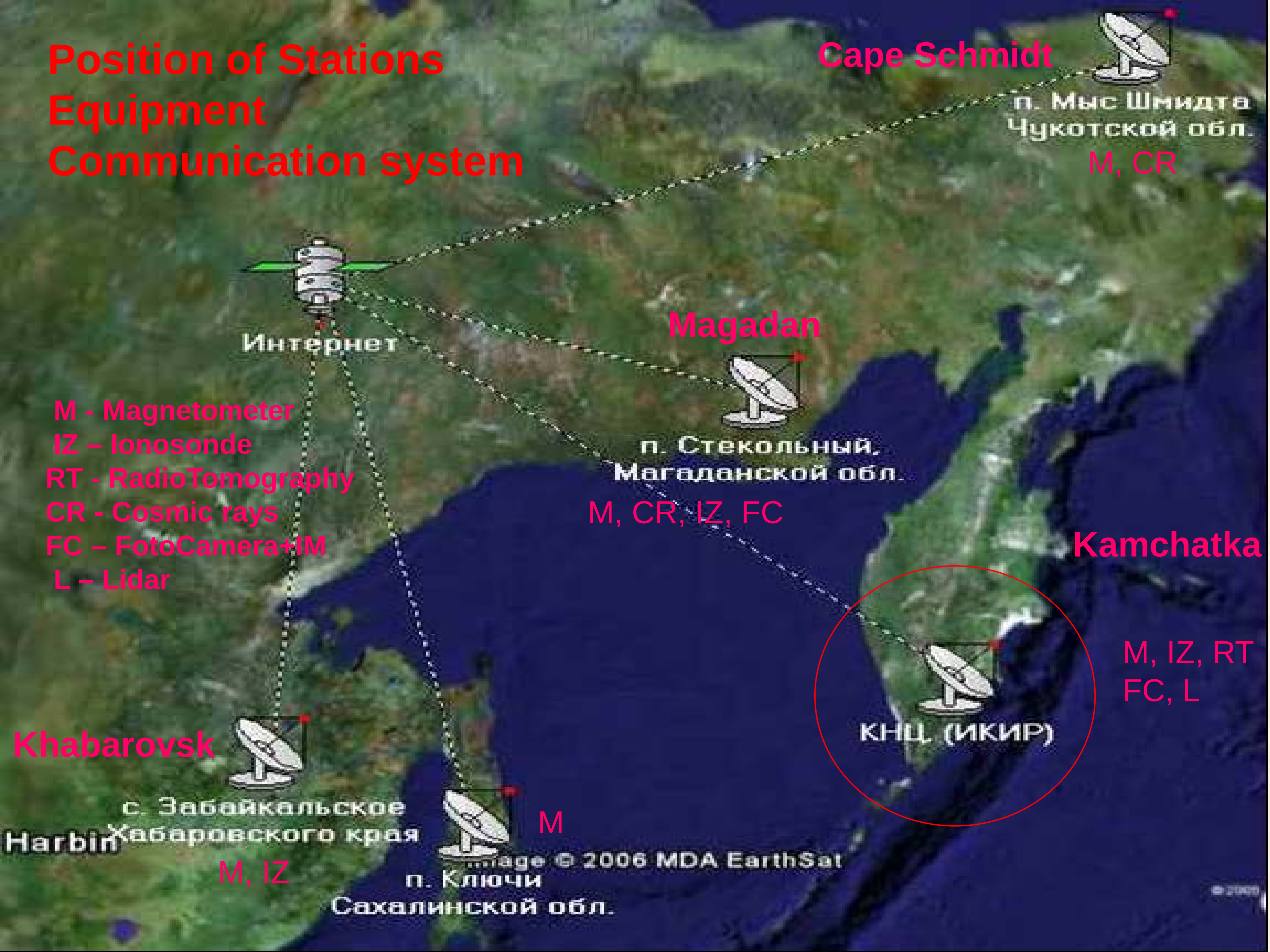

Magnetic observatories of IKIR FEB RAS

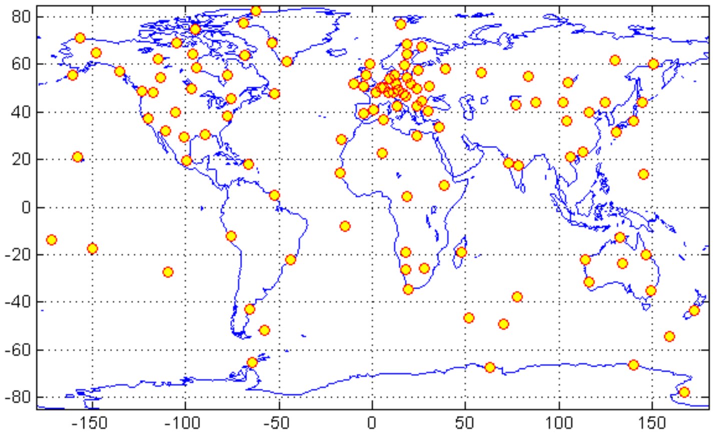

Magnetic observatories of INTERMAGNET (2012 г.)

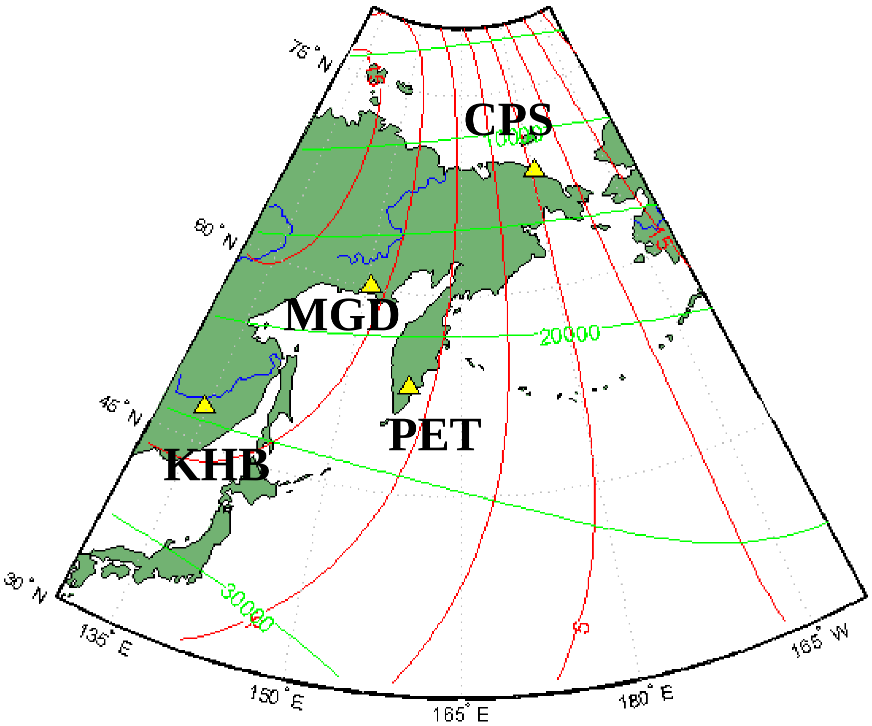

Observatory	start	IAGA	IMO	Geogr.		Geomag.	
“Cape Schmidt"	1967	CPS	-	68.9	180.6	64.0	231.5
“Magadan"	1965	MGD	2009	60.1	150.7	52.0	213.1
“Paratunka"	1968	PET	2013	53.0	158.3	45.8	221.5
“Khabarovsk"	1968	KHB	2013	47.7	134.7	38.4	202.5

Magnetic Systems on Far East

- 1. Russian (old and new Systems for keep succession)
- 2. Kyushu University, Japan
- 3. NICT, Japan
- 4. Nagoya University, Japan
- 5. Intermagnet

For what are so many Systems?

•For comparison

•For the Reliability of measurements

•For verifed data

Magnetic observatories of IKIR FEB RAS (equipment)

MGD – Magadan (2009):

variometers – FGE+GSM-90, MAGDAS, FRG, STELAB, dIdD

absolute – Theo 020, GSM-19, POS-1

PET – Paratunka (2013):

variometers – FGE+GSM-90, MAGDAS, FRG, STELAB, dIdD

absolute – LEMI-203, Mag-01H, GSM-19W, POS-1

KHB – Khabarovsk (2013):

variometers – Quartz-6, CAIS, dIdD

absolute – TT5, MMP-203, Mag-01H, GSM-19W, POS-1

CPS – Cape Schmidt (2016 - ?):

variometers – Quartz-3, MAGDAS, dIdD

absolute – MMP-203M2, Mag-01H, POS-1

Agreements with Japan (NICT, SERC - Kyushu Univ., STELAB – Nagoya Univ.)

Agreement with Germany (GFZ, Potsdam)

Updrade by Russian Academy of Sciences

Equipment according to INTERMAGNET Standards (year of joining)

dIdD-variometer GSM-19FD (GEM Systems, Canada)

Special small unheated hut for dIdD and its sensor inside
(GFO «Paratunka»)

Sensor of dIdD
GFO «Khabarovsk»

Sensor of dIdD
GFO «Magadan»

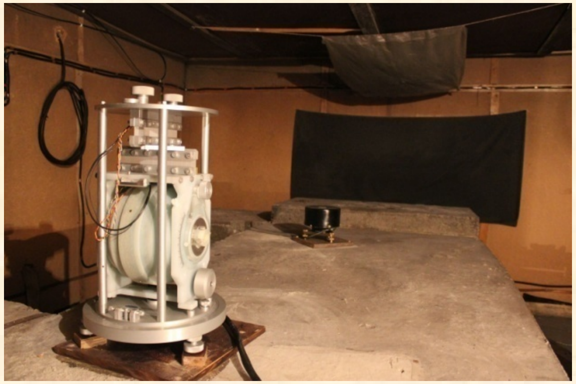

Sensor of dIdD
GFO «Cape Schmidt»

DI-fluxgate Mag-01H (Bartington Instruments Ltd., Great Britain)

Electronic unit (upper) and theodolite Wild-T1 with fluxgate sensor at GFOs "Paratunka" and "Khabarovsk"

Field observations of Sun (determination of azimuth of target) and declination-inclination measurements at station "River Karymshina" (Kamchatka)

International Agreements (Japan)

Sensors of magnetometers MAGDAS (lower) and FRG-601 (upper) at Paratunka

Recorded system of magnetometers MAGDAS (lower) and FRG-601 (upper)

Japanese colleagues check the MAGDAS system at Paratunka

International Agreements (GFZ, Potsdam)

Overhauser scalar magnetometer GSM-90 (sensor and console) – Paratunka, Magadan

Fluxgate 3-component magnetometer FGE - (Paratunka, Magadan)

Dr.H.-J.Linthe (GFZ) compare two scalar magnetometers (MMP-203 and GSM-19)

DIflux magnetometer at base of theodolite Zeiss-Jena Theo-020B (Magadan)

MAGDAS Magnetometer

MAGDAS Workshop on Kamchatka

Japan Systems on Far East

Magnetometer M
Ionosond IZ
FotoCamera FC
Induction Magnetometer IM

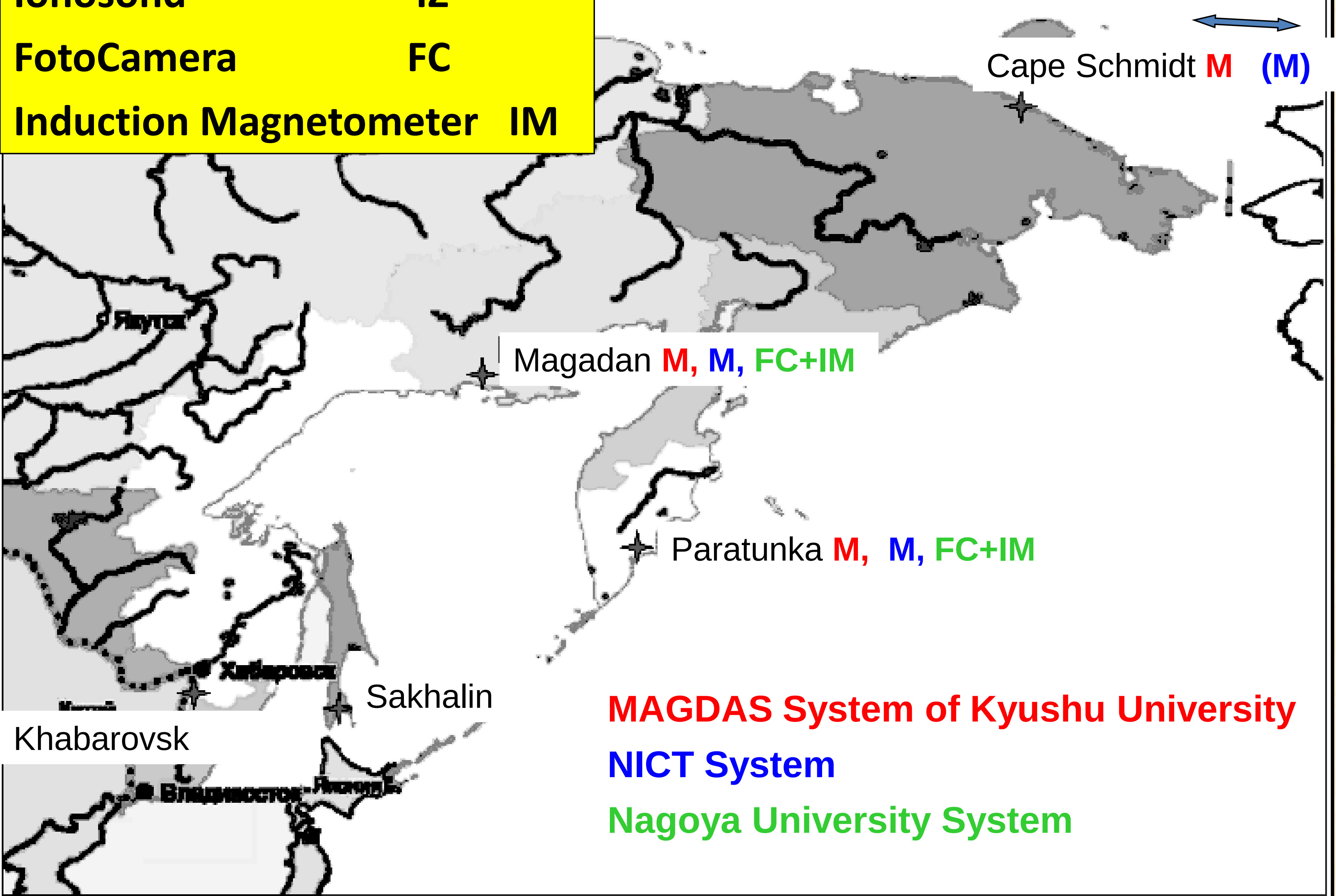

All-sky Airglow Imager System

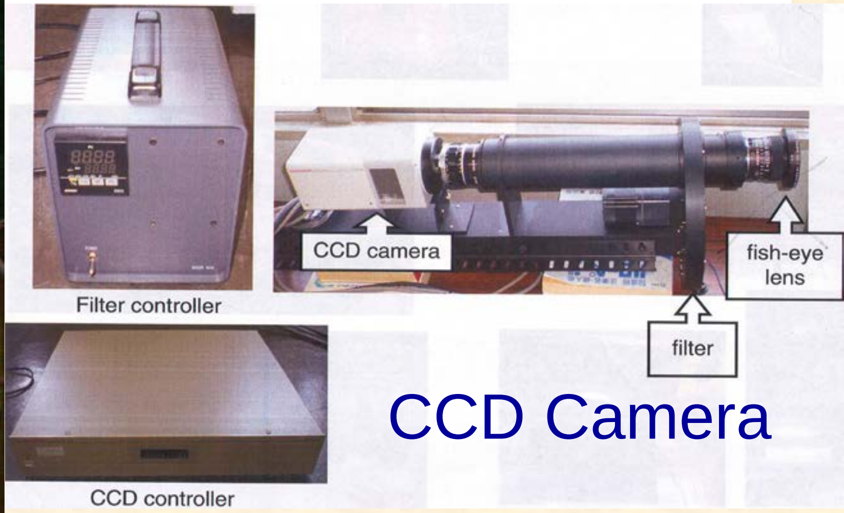

All-sky airglow imager system

ch 1. 557.7 nm, oxygen, 90-100 km
ch 2. 630.0 nm, oxygen, 200-300 km
ch 3. 700-1000 nm, OH-band, gydroxyl, 80-90 km
ch 4. 117.4 nm, oxygen, ~100 km
ch 5. 572.5 nm, (background)
ch 6. 486.1 nm, gydrogen, 300-400 km

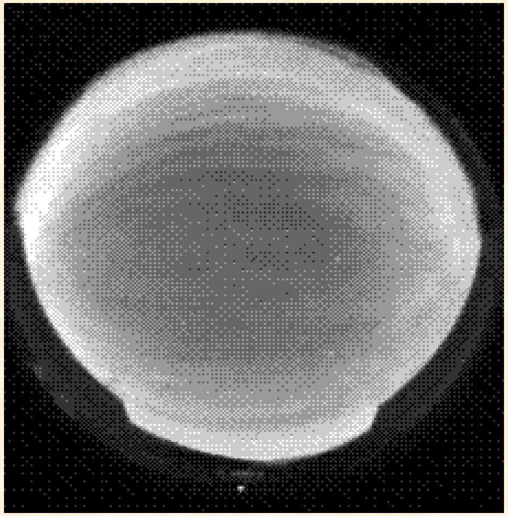

Internal gravity waves
H = 100km.
Paratunka
30.10.2007
Speed 70 - 100 m/s

ch 1. 557.7 nm, oxygen, 90-100 km

Radar Systems on Far East

Japan Doppler Radar FM-CW on Kamchatka

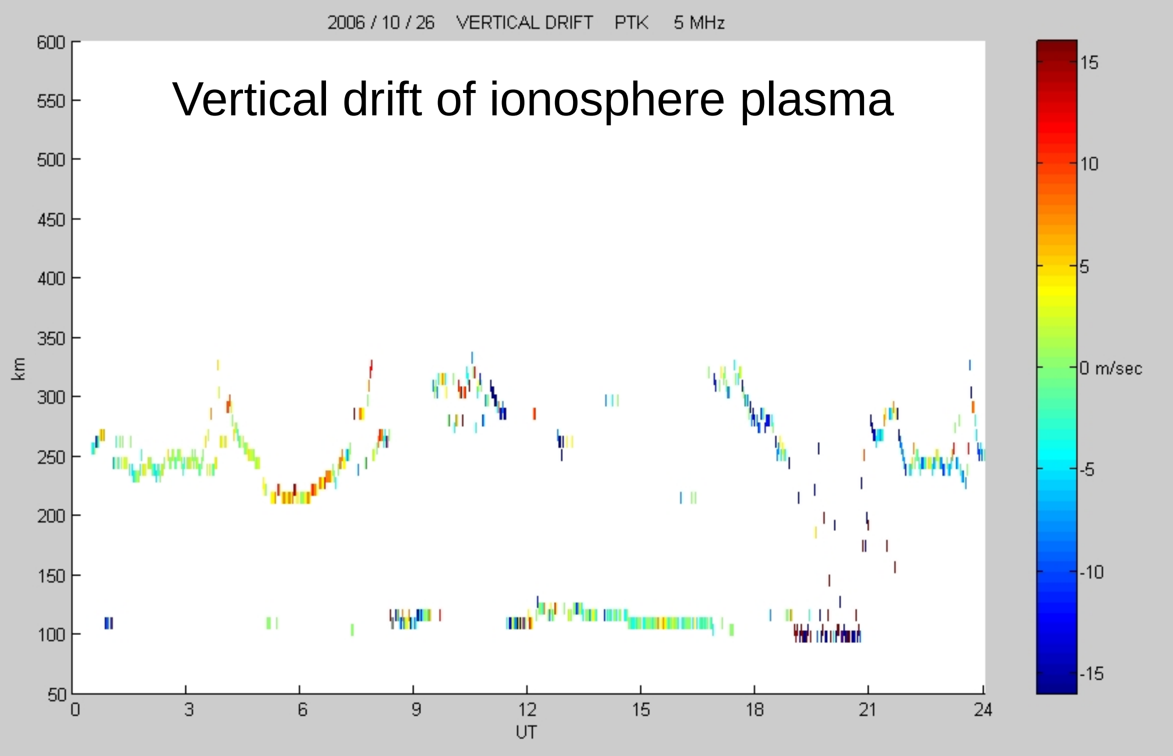

Russian Ionosonde

Ionosond Systems on Far East

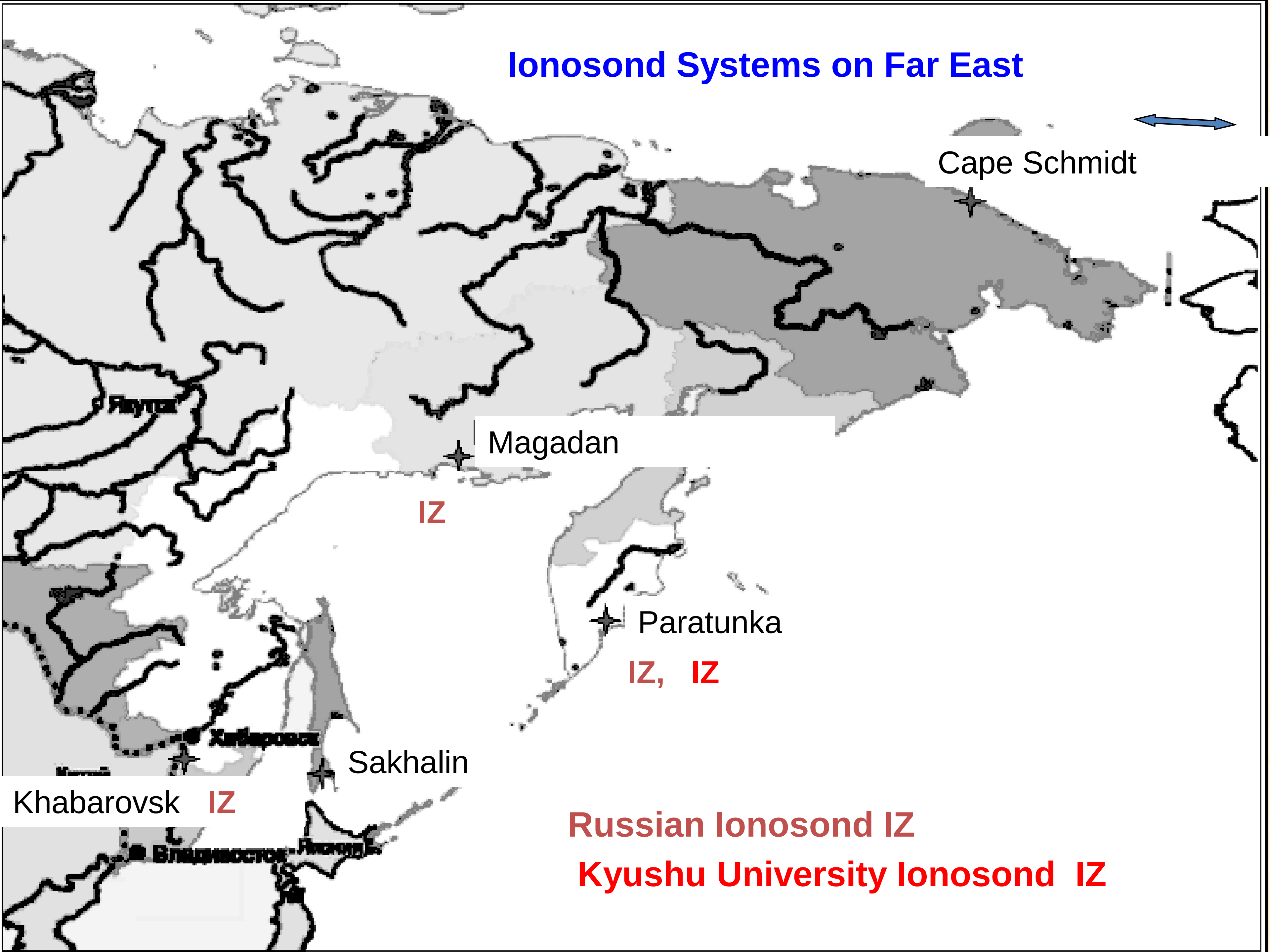

The complex analysis of the magnetic storm on August 3 and 4, 2010 (Paratunka data)

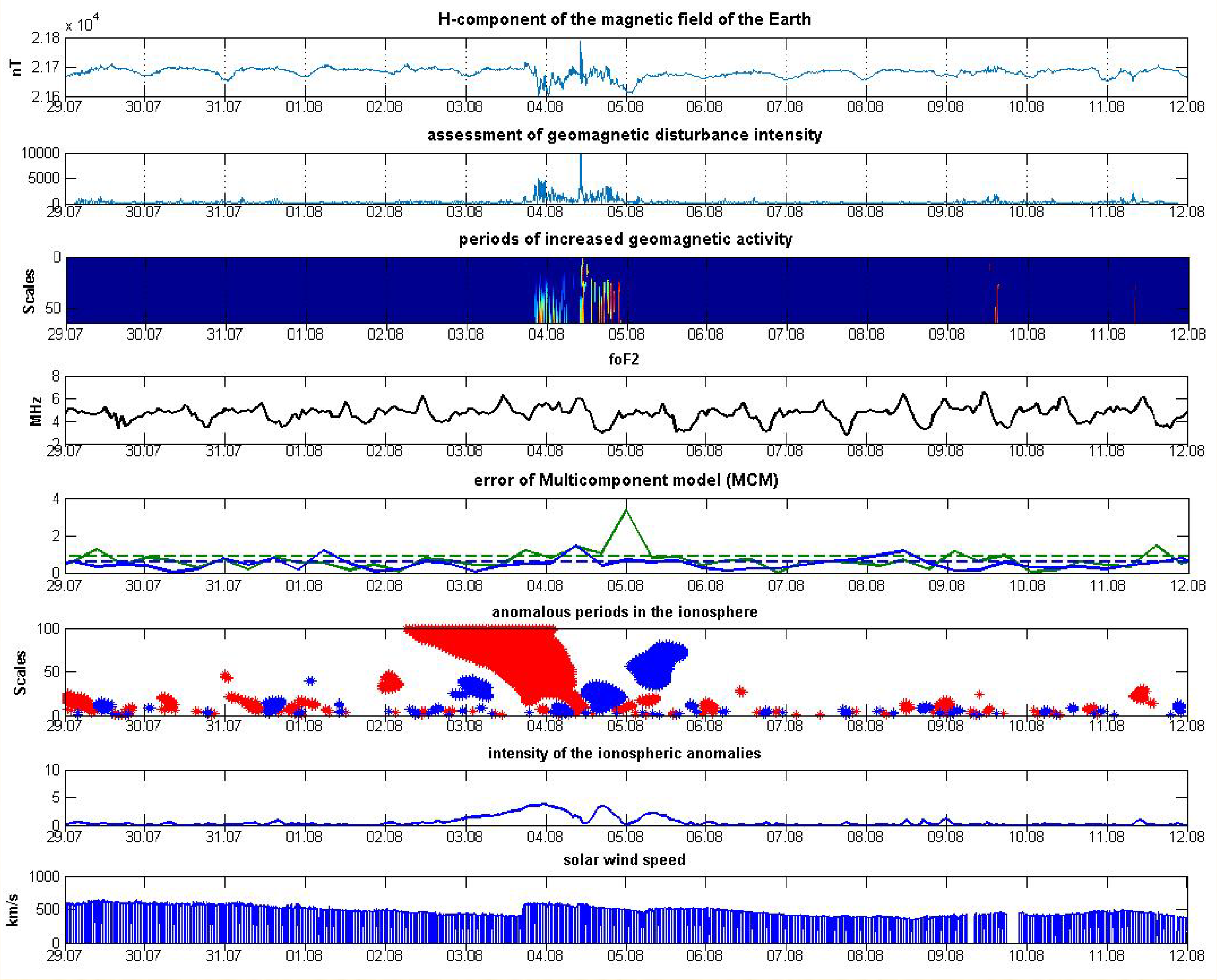

The magnetic storm on March 7-8, 2012 (Paratunka data)

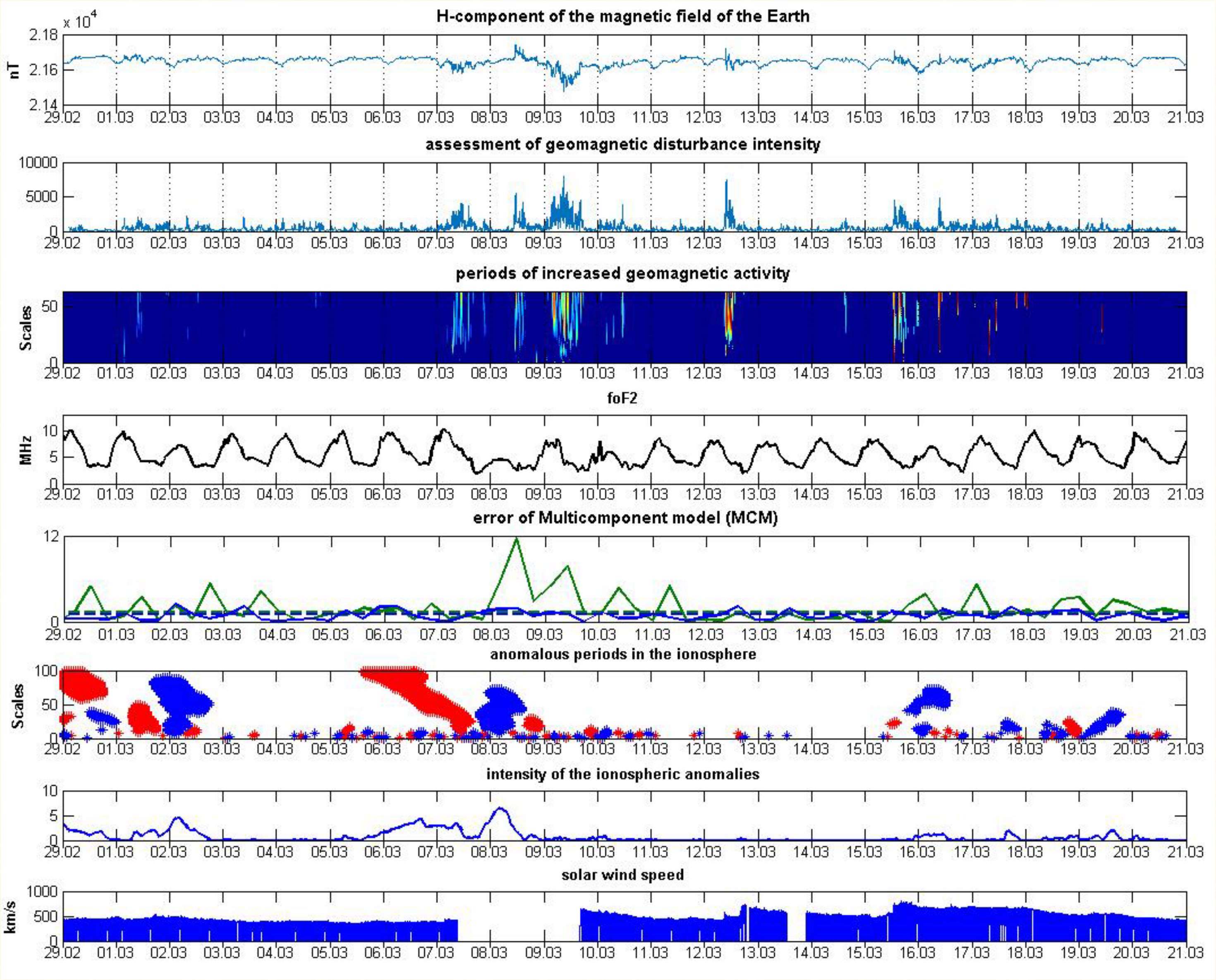

Radiotomography of Ionosphere by signal of low orbit satellite

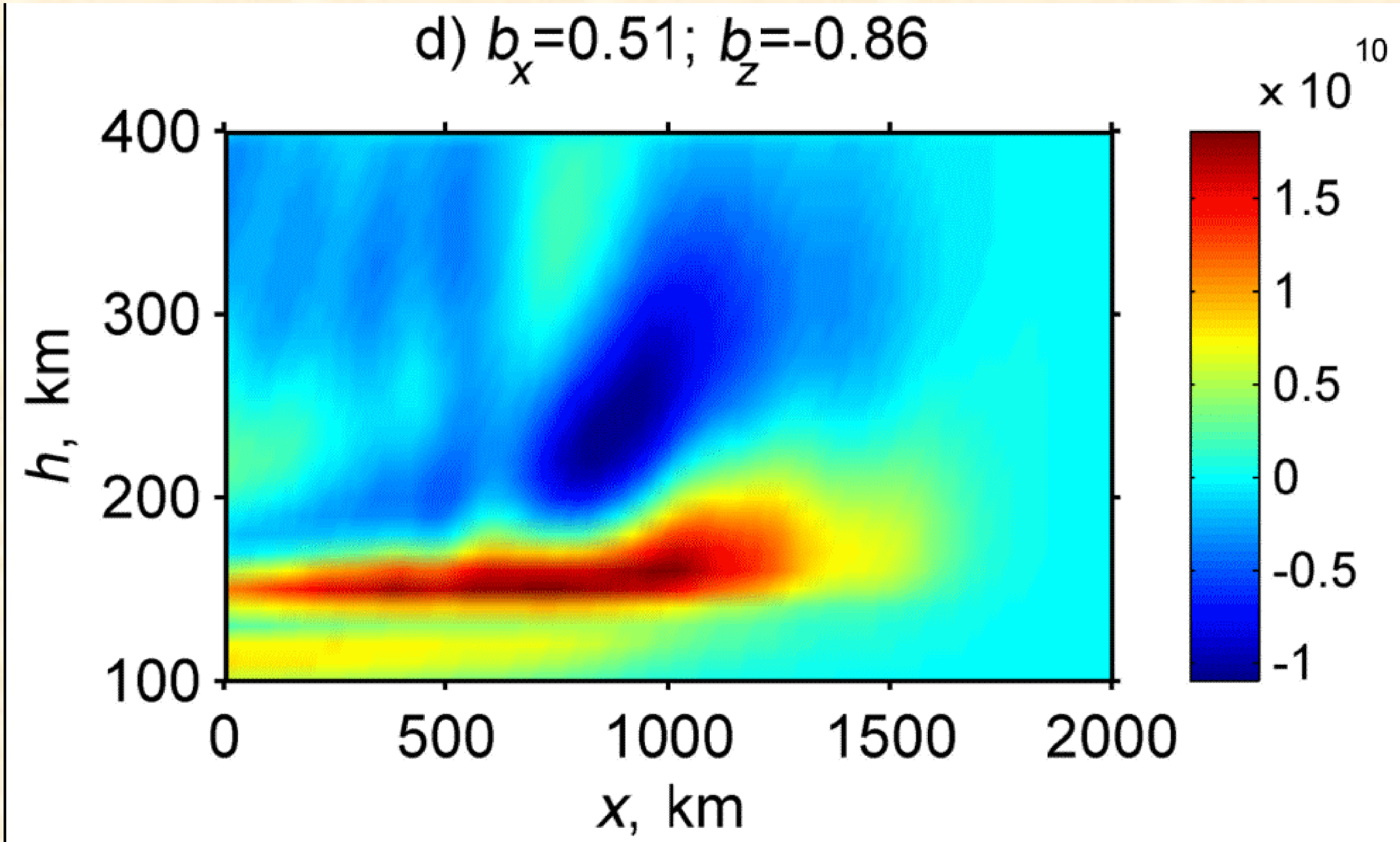

Radiotomography of Ionosphere by GPS signal

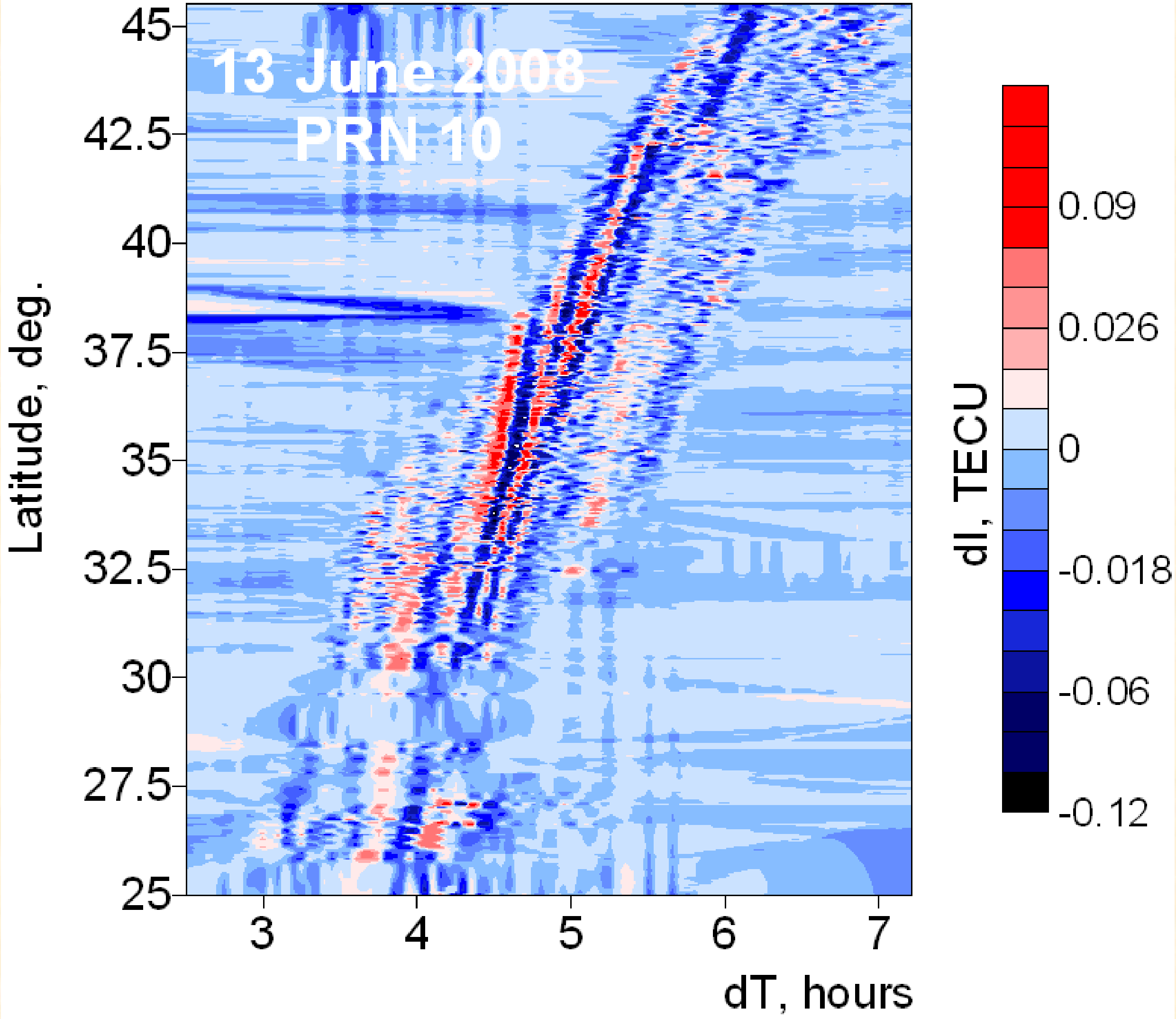

Cosmic Ray System on Far East

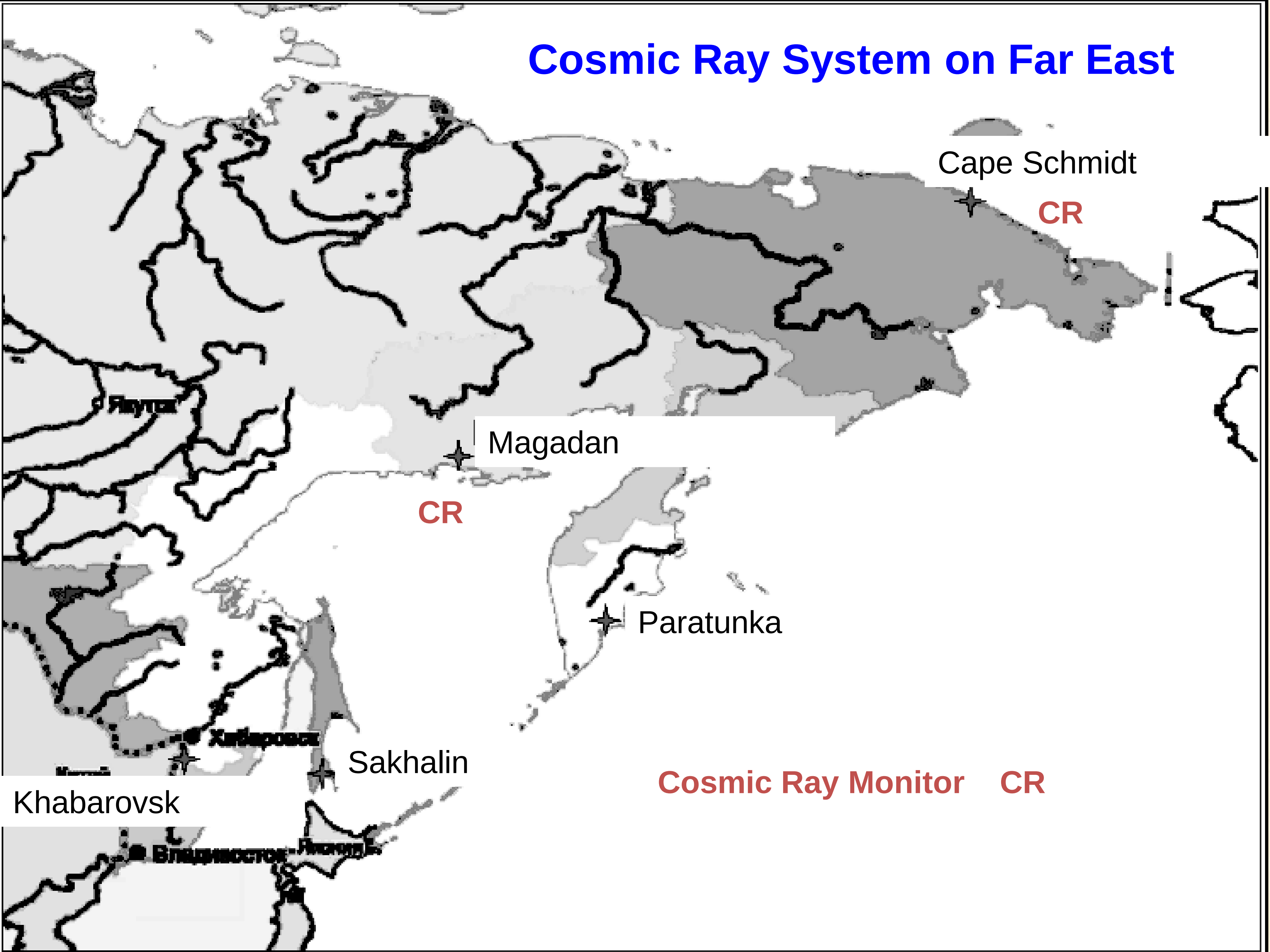

Cosmic rays monitor on Cape Schmidt

Multi scale wavelet decomposition of the cosmic rays signal

By performing multiresolution wavelet decomposition of the function $f_0(t)$ to the level m we obtain its representation in the following form:

$$f_0(t) = g_{-1}(t) + g_{-2}(t) + \ldots + g_{-m}(t) + f_{-m}(t) = \sum_{j=-1}^{-m} \sum_{n} d_{j,n} \Psi_{j,n}(t) + \sum_{n} c_{-m,n} \varphi_{-m,n}(t)$$

g_j - detailed components, j - scale

f_{-m} - trend component

$c_{-m,n} = \langle f, \varphi_{-m,n} \rangle, \; d_{-m,n} = \langle f, \Psi_{-m,n} \rangle$

$\phi_{j,n}(t) = 2^{j/2} \phi(2^j t - n)$ - scaling function

$\Psi_{j,n} = 2^{j/2} \Psi\left(2^j t - n\right)$ - wavelet basis

On the basis of analysis of the data of cosmic rays for the period from 2001 to 2014, it is revealed that m = 6 is the best level of decomposition for signal analysis on the basis of neural network.

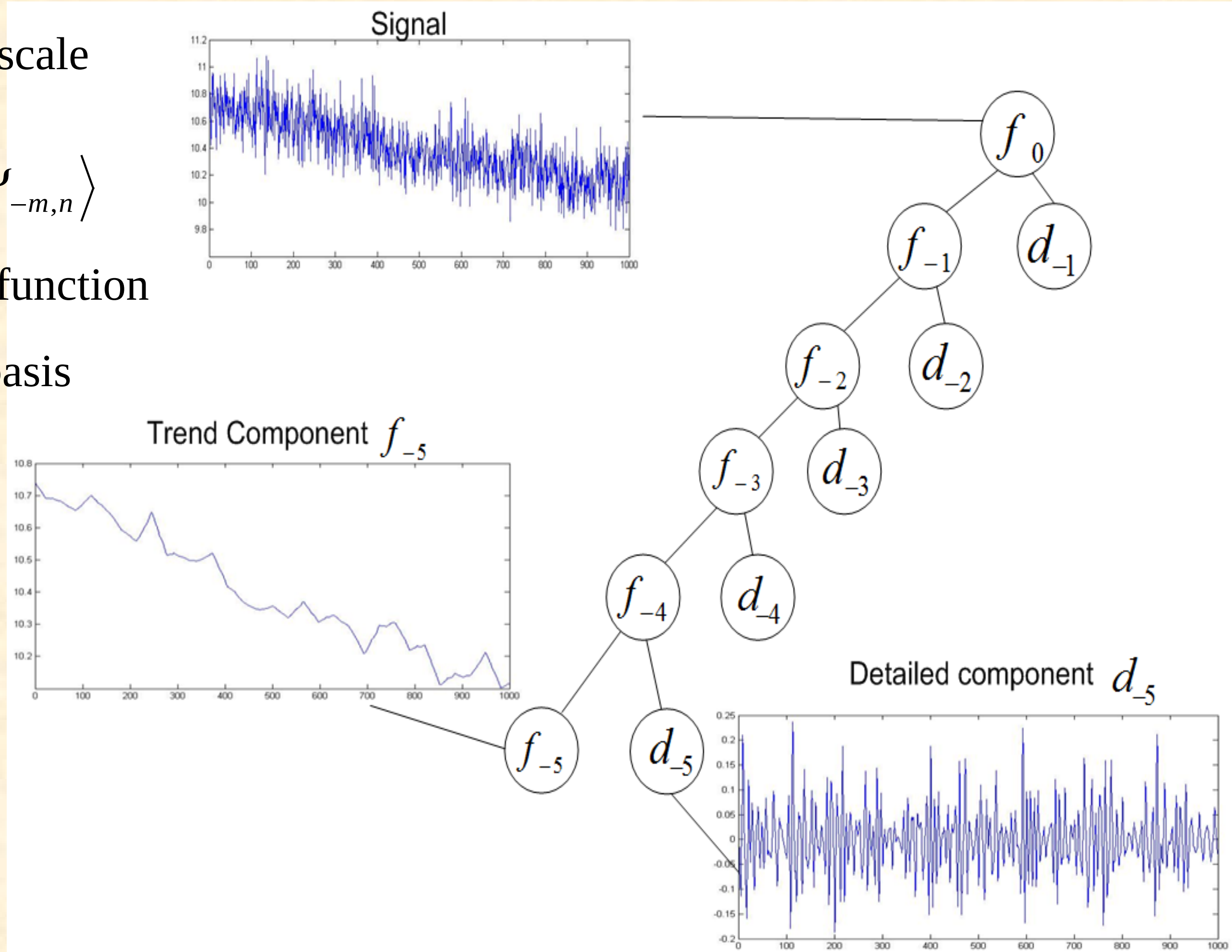

Approximation of the trend component on the basis of neural network

Constructed neuron networks performs a one-step data prediction of the trend component. The training set is formed from the data registered during quiet periods. In this case, the trained neural network reproduced regular variations of the data being approximated, which is typical for quiet conditions. Network training was performed on the basis of the back error propagation algorithm.

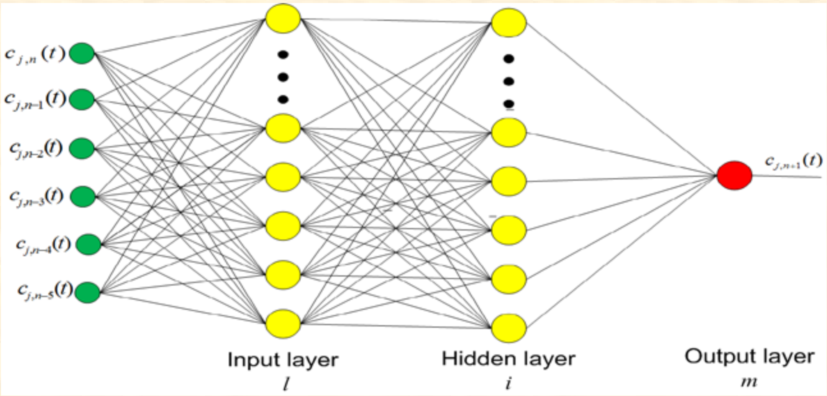

$$c_{j,n+1}(t) = \varphi_m^3\left(\sum_i \omega_{mi}^3 \varphi_i^2\left(\sum_l \omega_{il}^2 \varphi_l^1\left(\sum_n \omega_{\ln}^1 c_{j,n}(t)\right)\right)\right),$$

$$\phi_l^1(z) = \phi_i^2(z) = \frac{2}{1+\exp(-2z))} - 1 \quad \varphi_m^3(z) = a * z + b$$

$\omega_{\ln}^1$ - the weight of the connection between input n and neuron l of the input layer of network

ω_{il}^2 - the weight of the connection between neuron l of the input layer of network and neuron i of the hidden layer of network

ω_{mi}^3 - the weight of the connection between neuron i of the hidden layer of network and neuron m of the output layer of network

Network error at time moment t_n : $e_m[t_n] = \left| f_{0,i}^{*(-m)}[t_n] - \hat{f}_{0,i}^{*(-m)}[t_n] \right|$

$f_{0,i}^{*(-m)}[t_n]$ - desired output, $\hat{f}_{0,i}^{*(-m)}[t_n]$ - actual output,

Anomalous changes occur when $E_{m,U} = \frac{1}{U}\sum_{n=1}^{U} e_m[t_n] > T$

U - the length of the observation window,

T - some preassigned threshold.

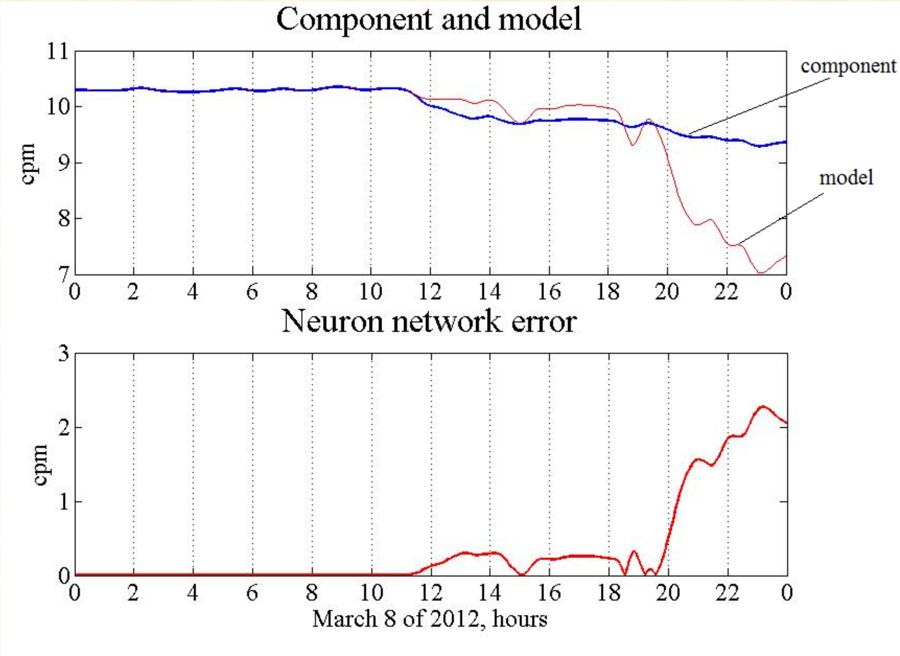

Detailed analysis of cosmic ray intensity variations during the magnetic storm on March 7-8, 2012

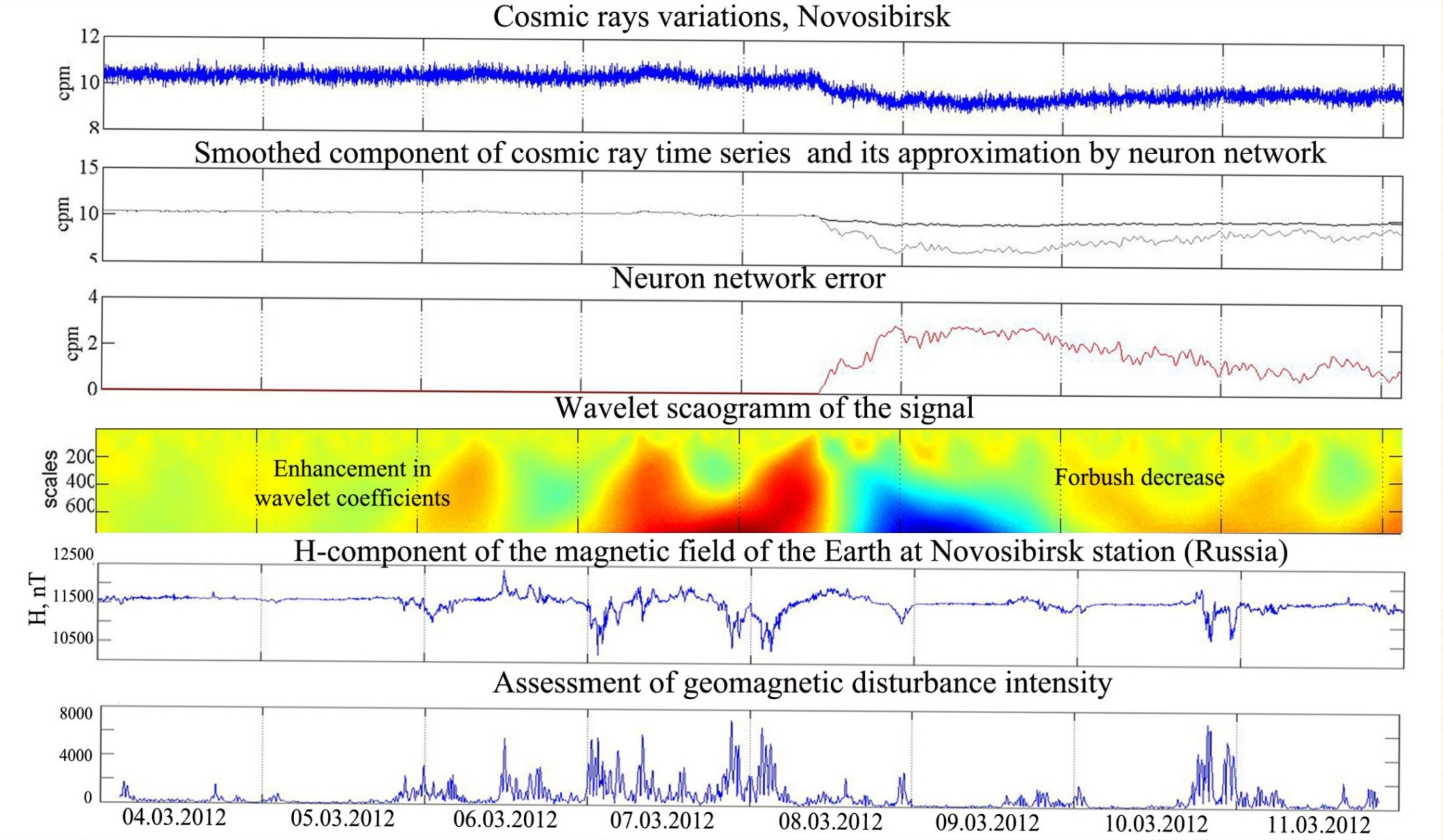

AWDANet System on Far East for magnetosphere diagnostic

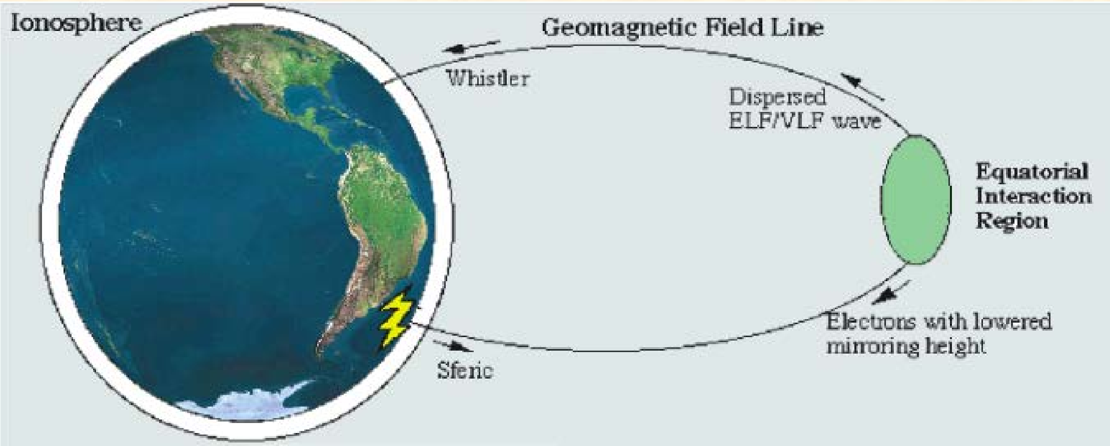

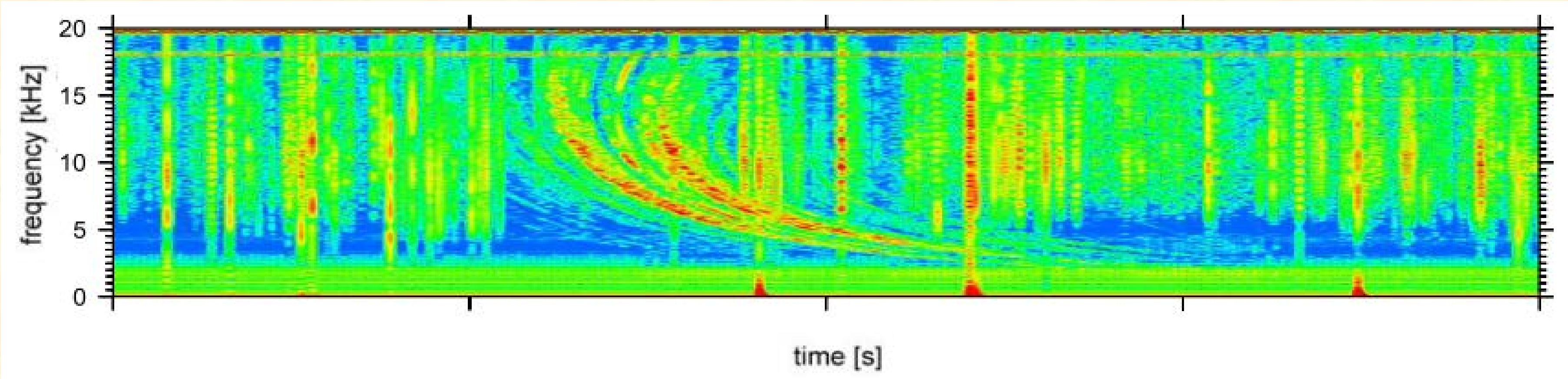

Automatic Whistler Detector and Analyzer systems' network (AWDANet, J. Lihtenberger)

http://plasmon.elte.hu/

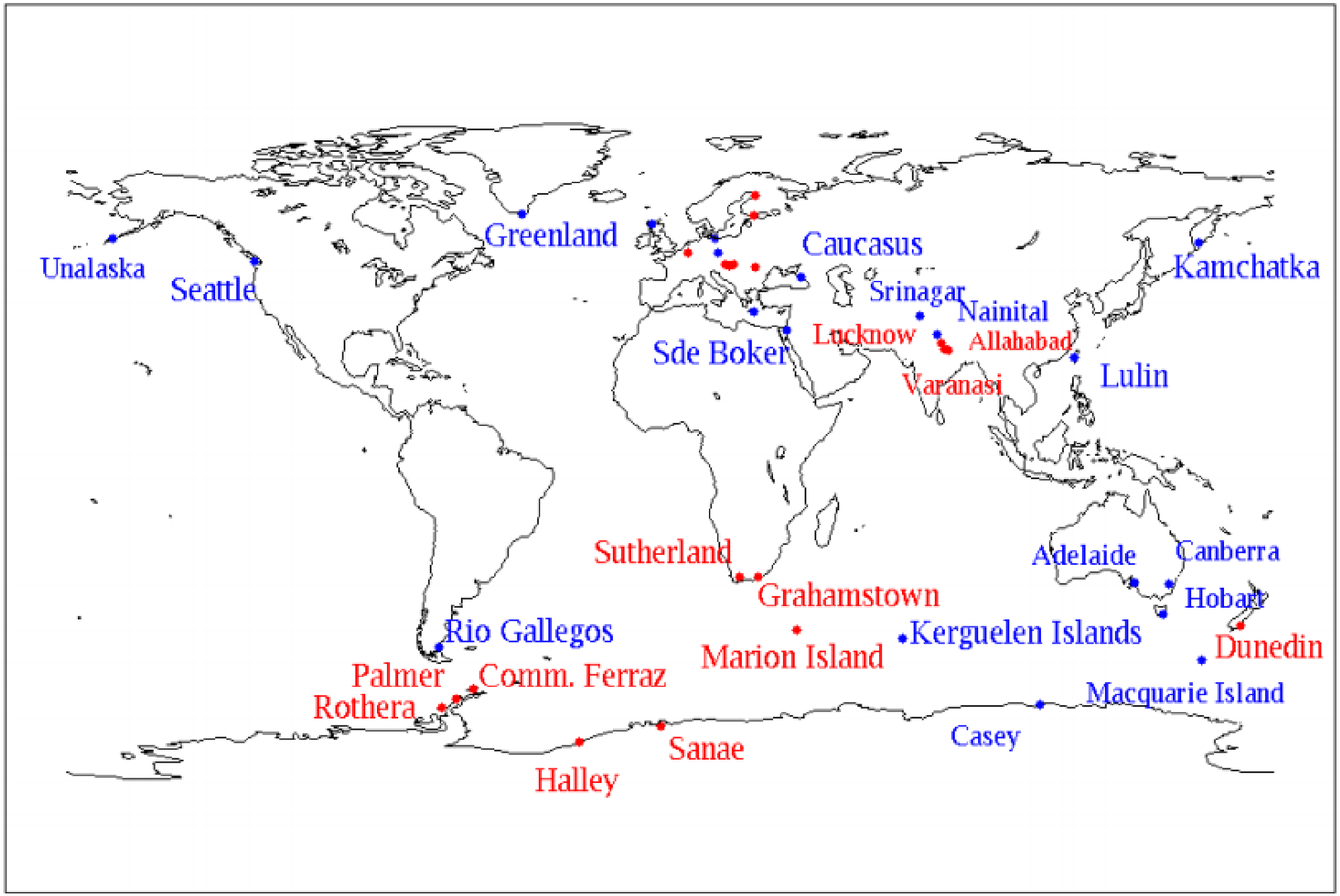

Whistlers and Lightning observation System on Kamchatka

SuperDARN on Far East

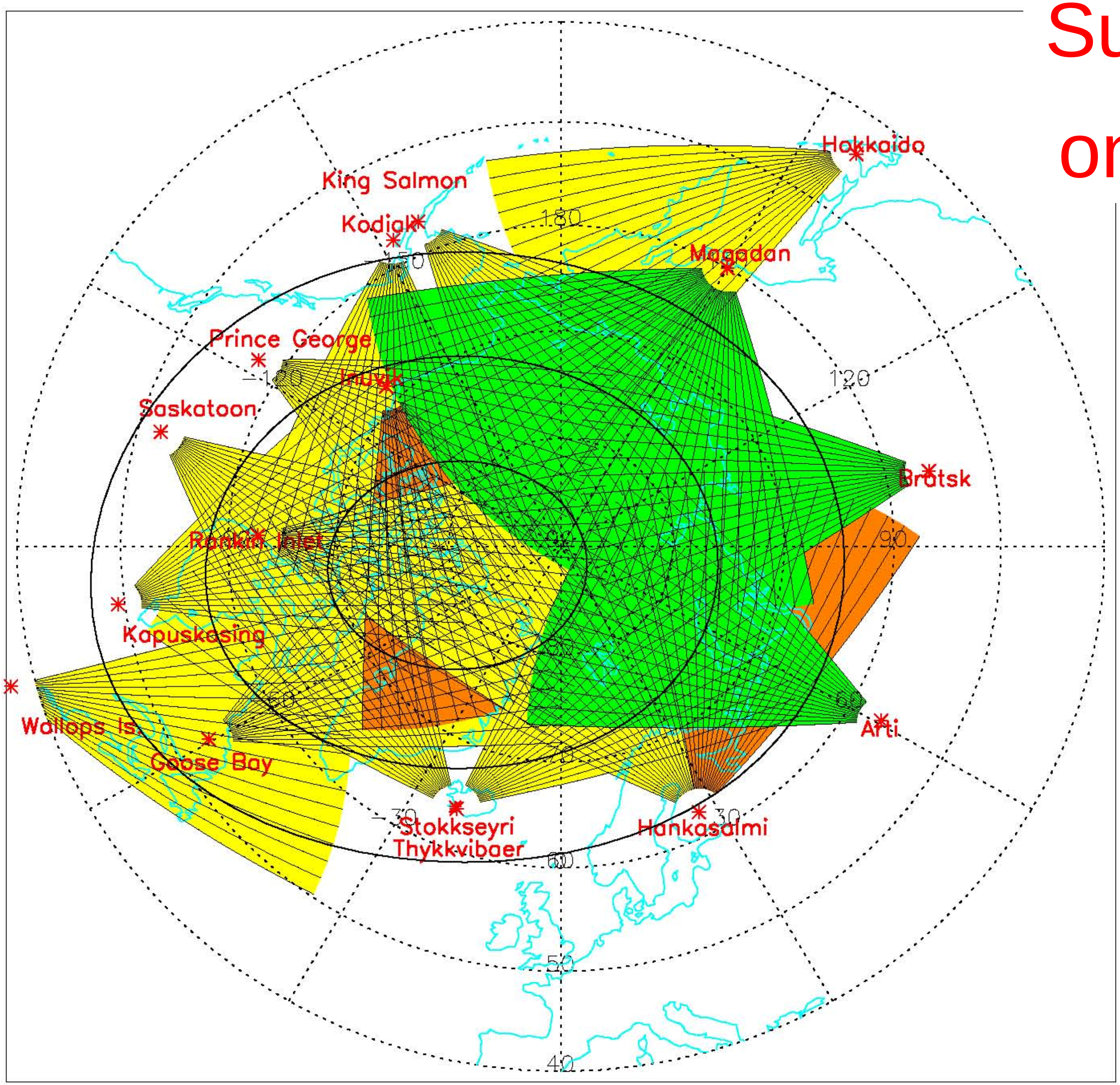

Facilities of magnetosphere and ionosphere diagnostic

- Magnetometers
- Ionosonds
- Radiotomography
- AWDANet
- SuperDARN
- Imager of night sky
- Lidar System

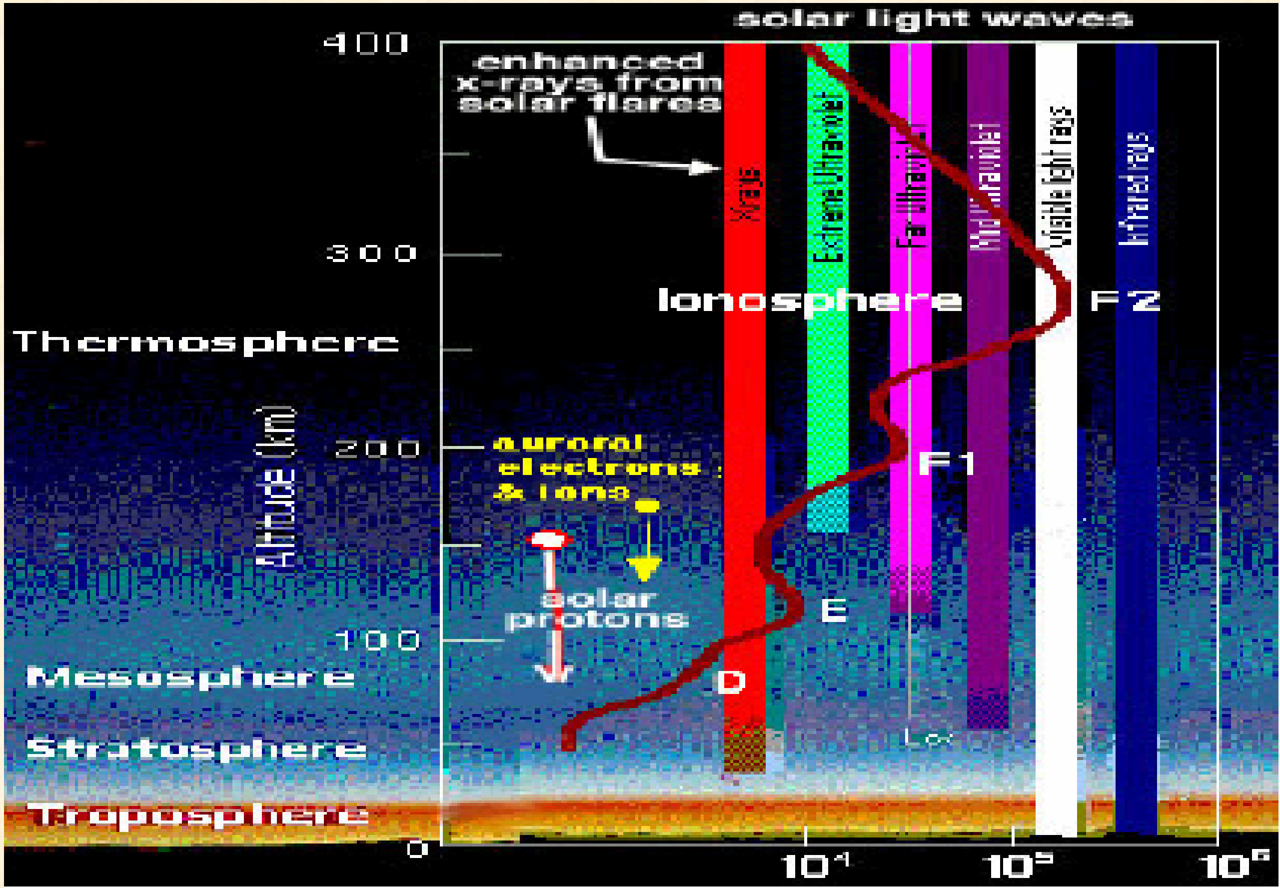

Lidar System

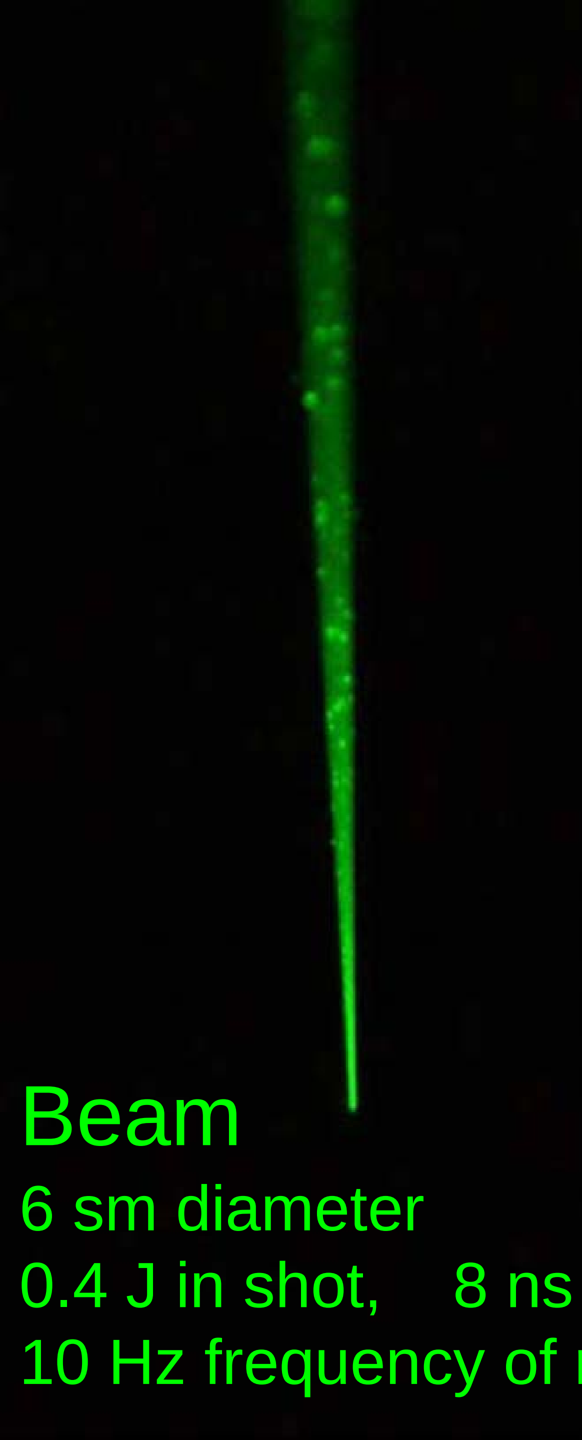

Laser

Nd in YAG

Second harmonic

Beam

6 sm diameter

0.4 J in shot,   8 ns duration

10 Hz frequency of repetition

Transmitter 1: Laser Quantel Brilliant-B (Nd in YAG)

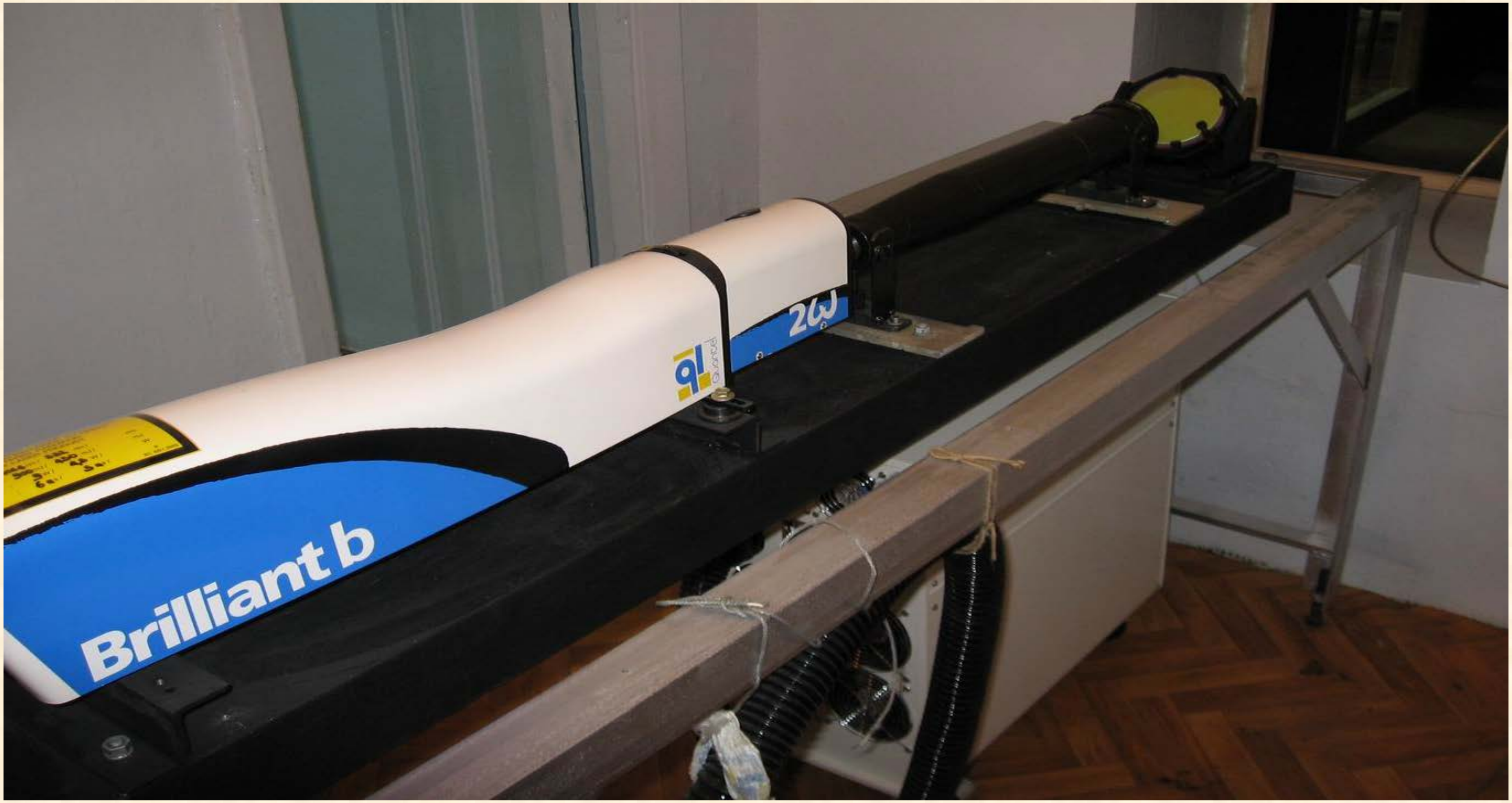

- Energy – 400 mJ, Wavelength – 532 nm
- Repetition rate – 10 Hz
- Beam after collimator - 6 sm

- Laser YG-980 with energy in an impulse 2500 mJ (the first harmonic), 1250 mJ (the second harmonic), 800 mJ (the third harmonic),
- The dye laser pumped by the second and third harmonic of laser YG-980, changing of frequency in a visible range, energy in an impulse up to 200 mJ.

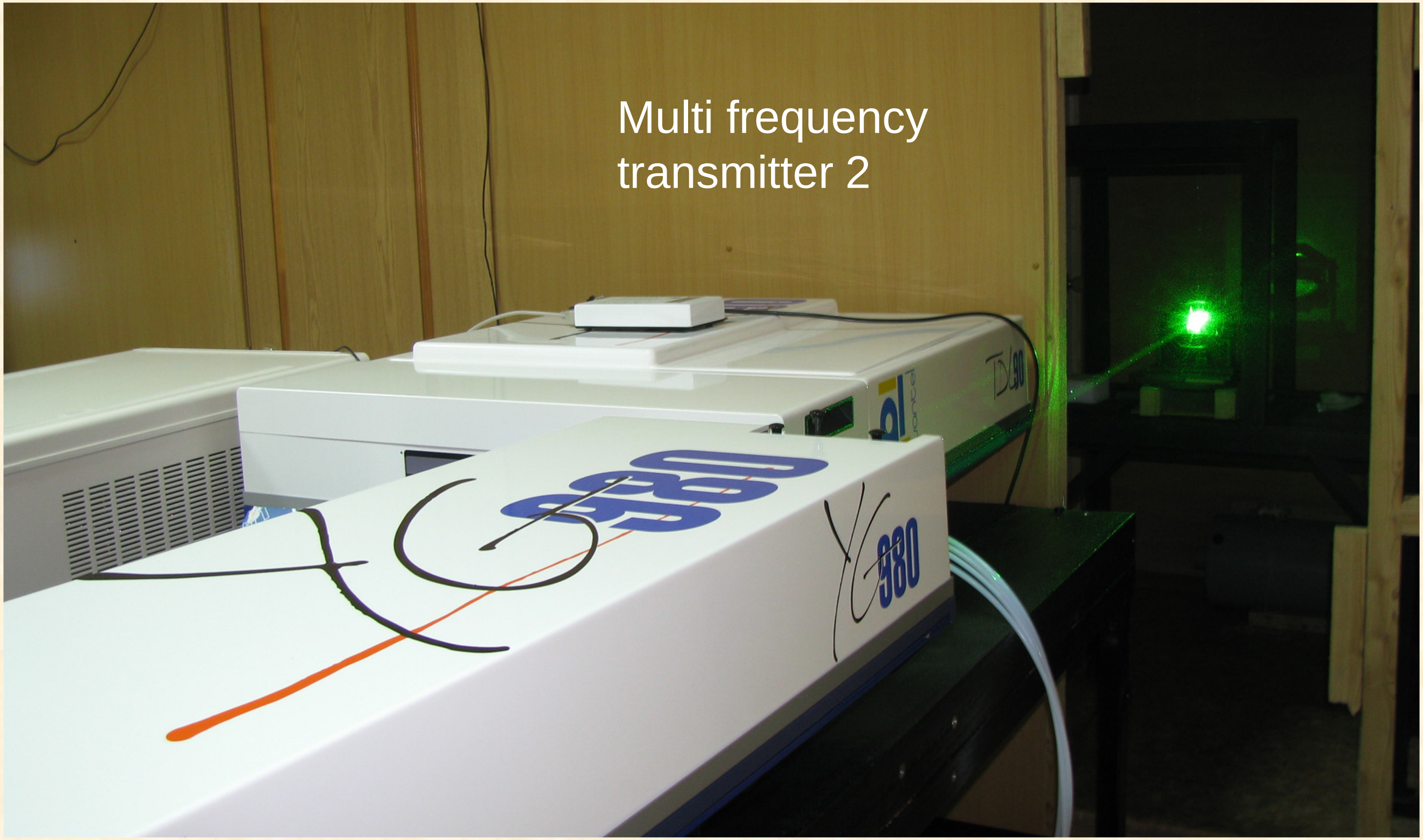

Lidar telescopes

diameter of mirror – 60 sm

focus length – 210 sm

diameter of mirror – 25 sm

focus length – 150 sm

The photon counter and spectrum analyzer of optical radiation Spectra Pro 2500i, the CCD chamber with the amplifier of brightness PicoStar UF-12QE

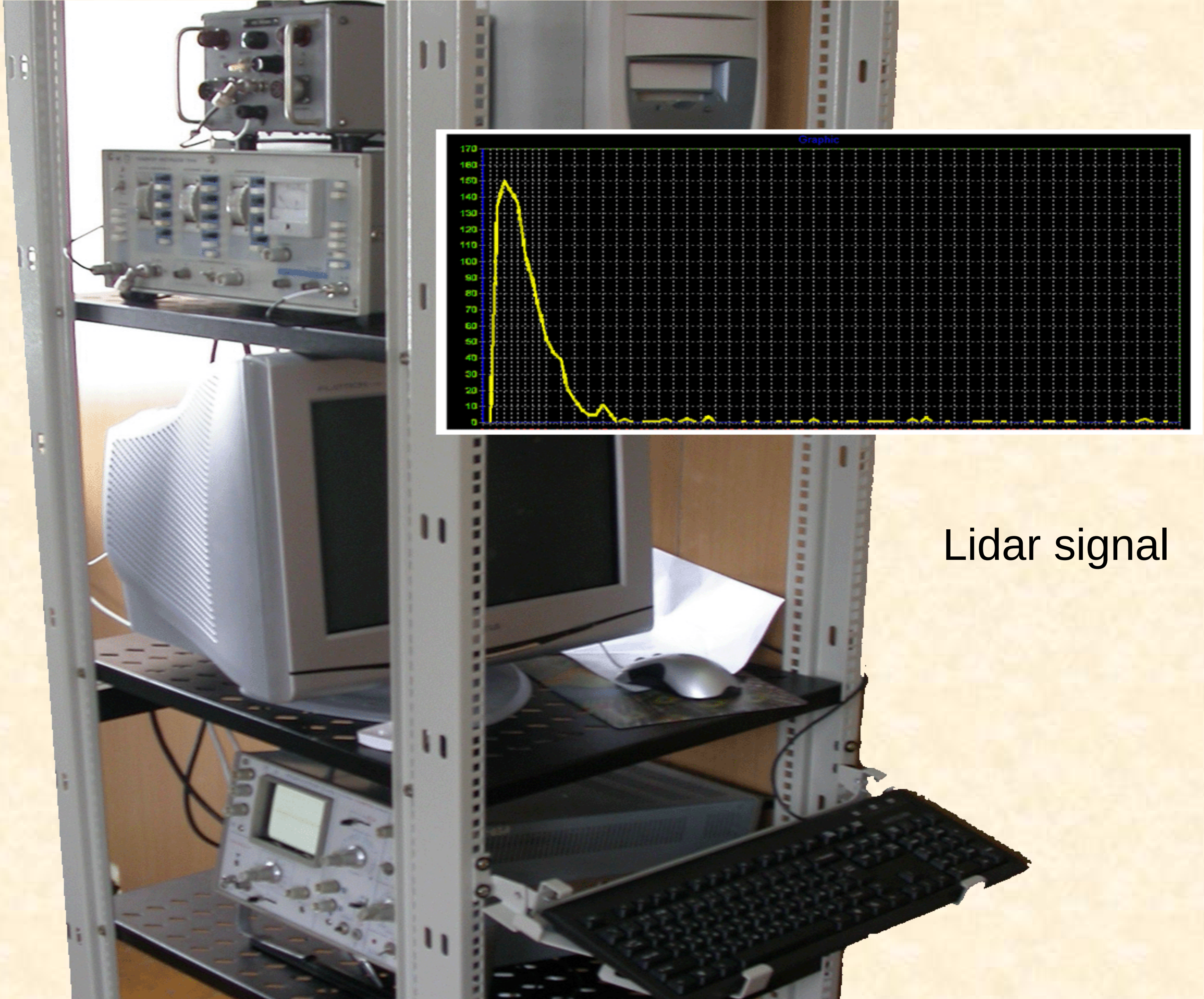

Lidar signal

Example of diagram during precipitation of charge particles

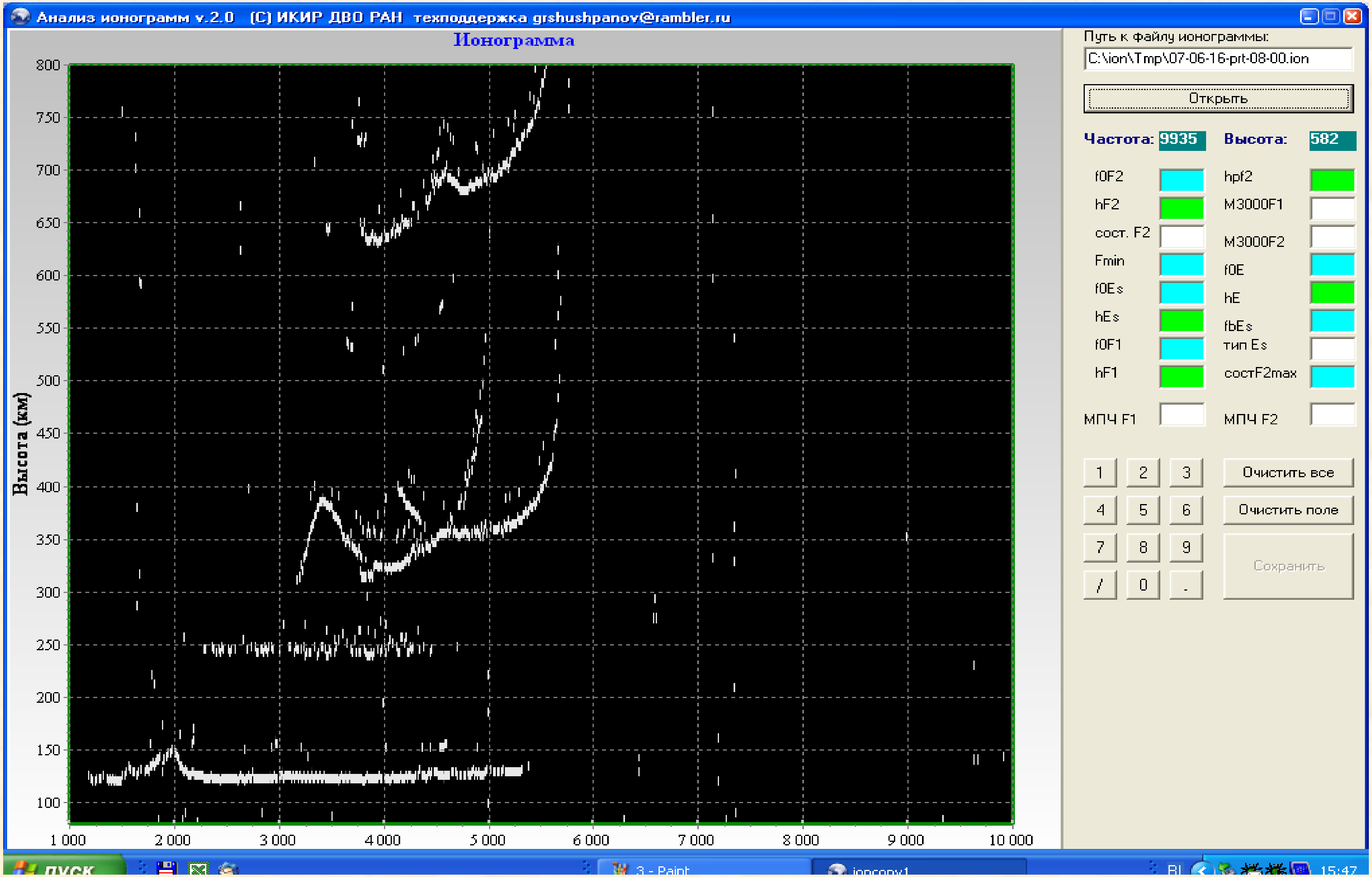

Results of observations on 28 March 2008

(Bychkov and Shevtsov 2012)

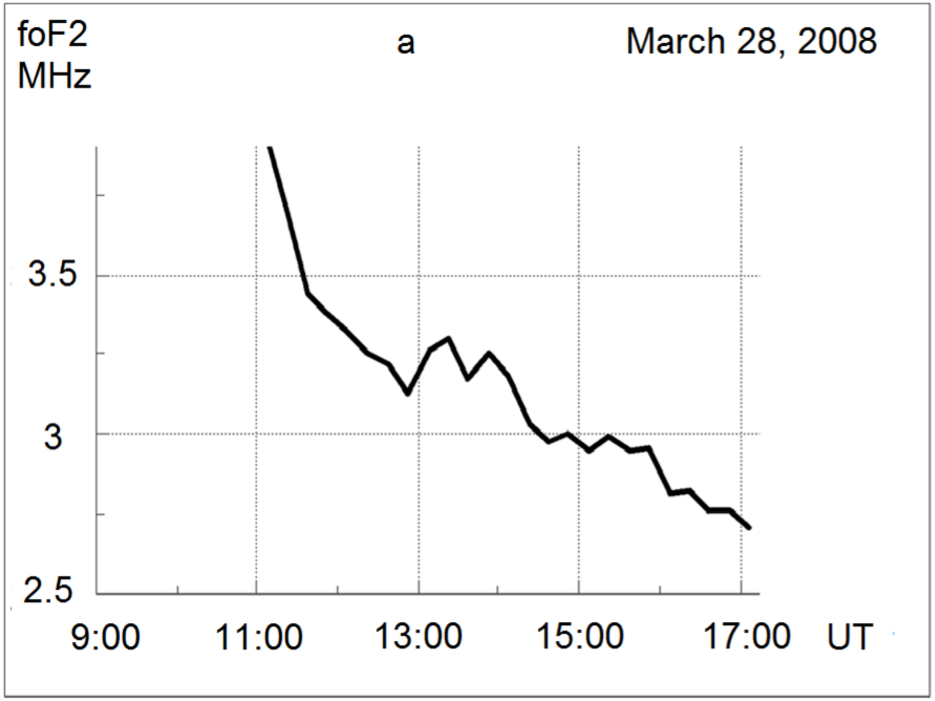

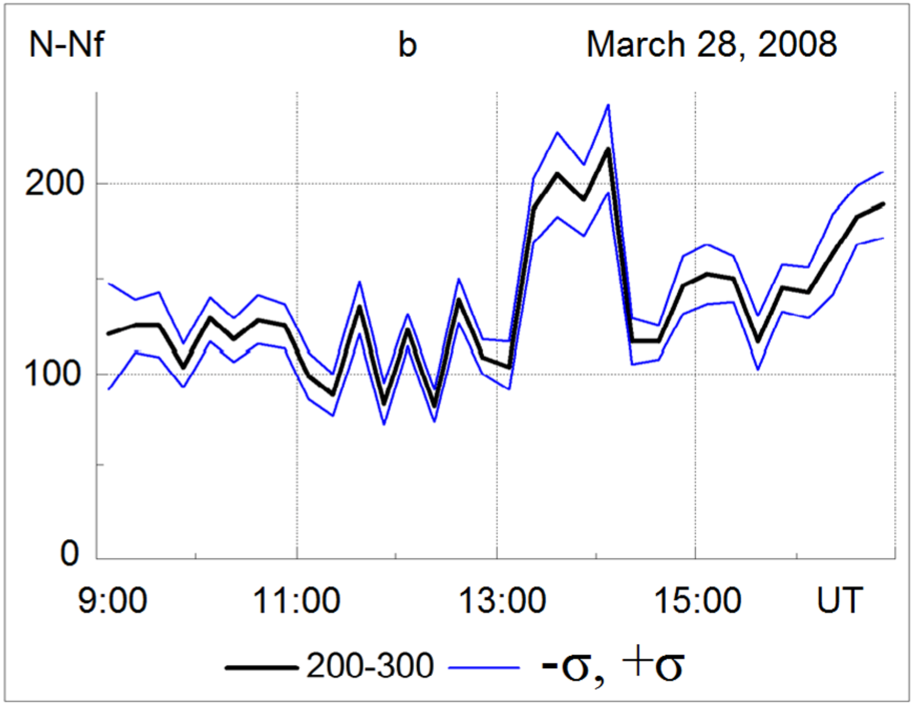

- Critical frequency foF2 of the ionosphere F2 layer (*a*);
- lidar signal N–Nf summed for altitudes 200-300 km representing the total number of detected photons minus the background level (*b*).
- The middle curve shows the average signal, the upper and lower curves illustrate the standard deviations.
- The accumulation of lidar signal is 15 minutes.

Results on 6 September 2008

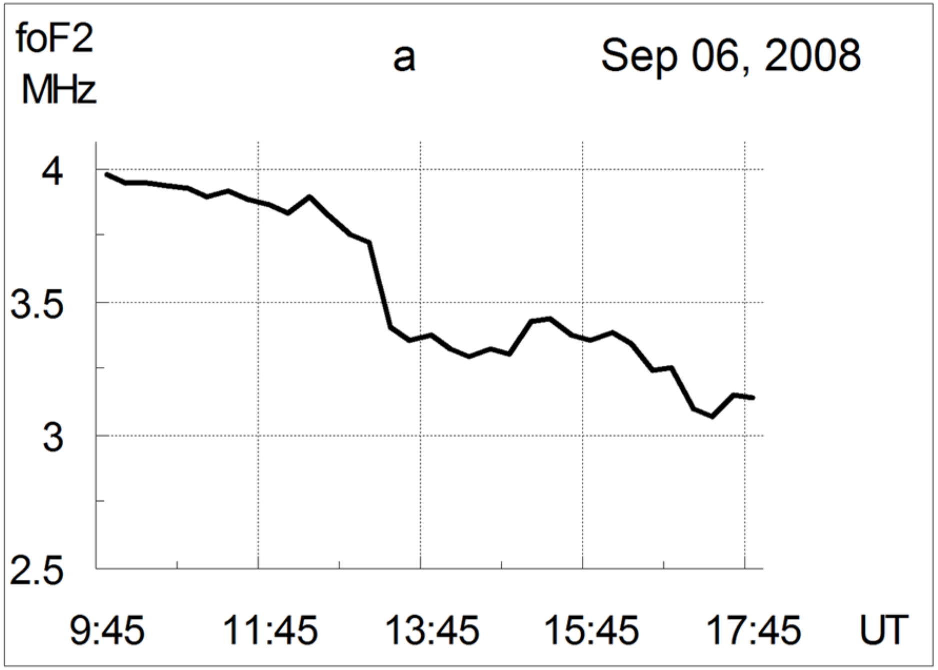

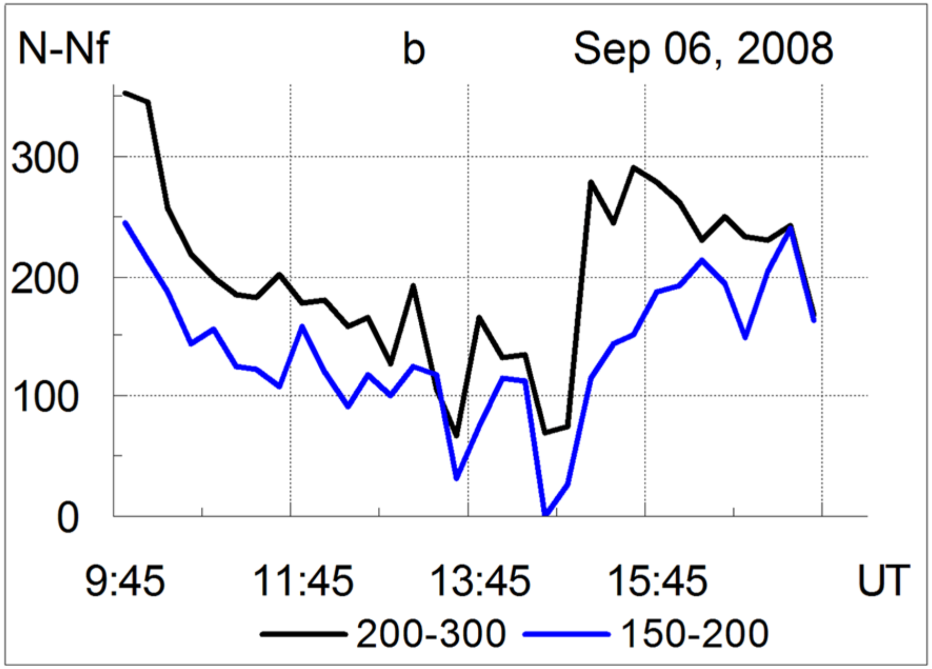

- Critical frequency foF2 of the ionospheric F2 layer (*a*)
- lidar signals summed for altitudes 150–200 and 200–300 km (*b*).

Luminescence specters of the night sky on February, 28th 2012 due to precipitations from the radiation belts have a great variability

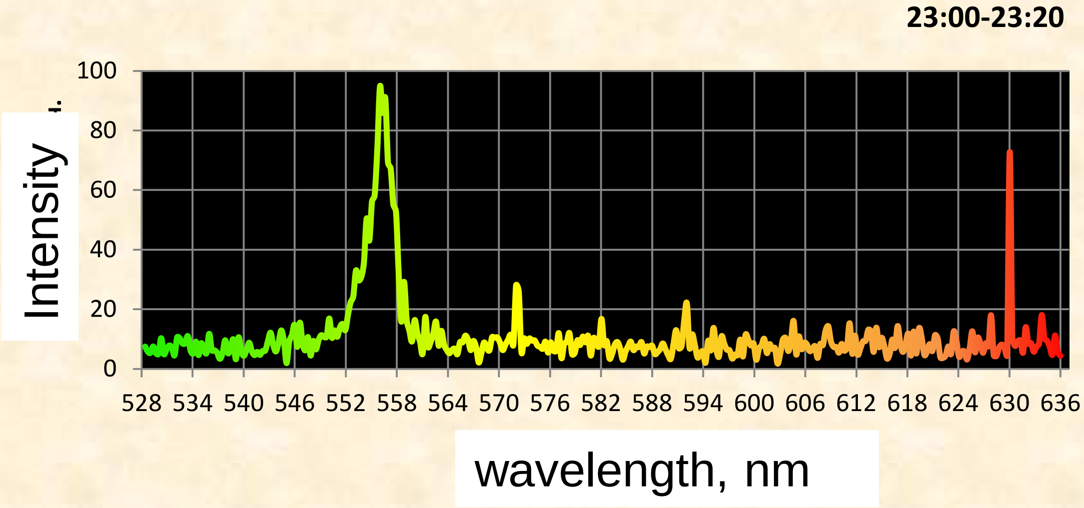

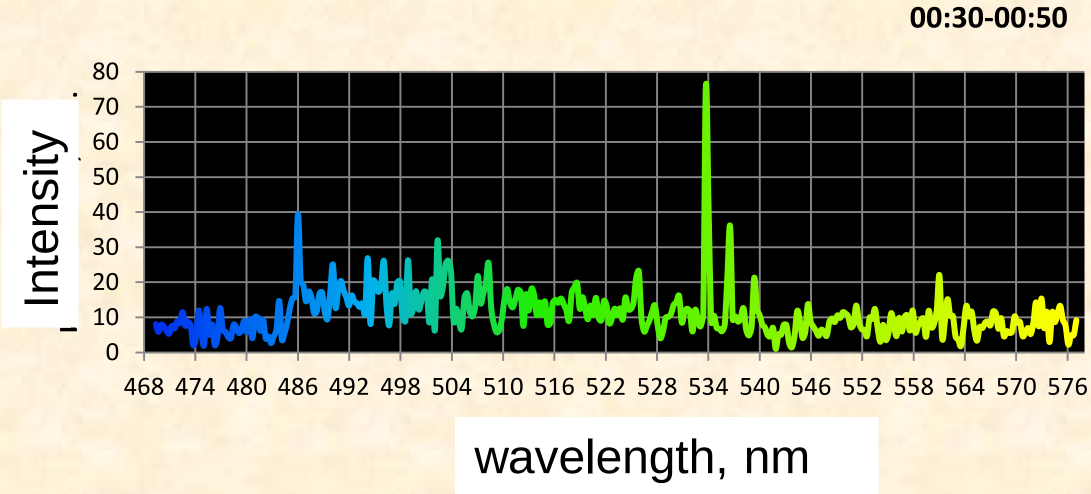

- There was a quiet magnetic condition.
- All K-indexes were

  equaled 1.

Spectral lines of the nitrogen atom ions transitions lie within the band of second harmonic of the Nd: YAG laser 532.08 ± 0.07 nm

Example of spectral lines of atomic transitions from Catalog NIST ASD, 1978

		Wavelength in Air (nm)	A_{ki} (s^{-1})	Lower Level	Term	J	Upper Level	Term	J
1	NII	532.0202	4.20e+07	$2s2p^2(^4P)3p$	$^5P°$	2	$2s2p^2(^4P)3d$	^5P	1
2	NIII	532.087	5.68e+07	$2s2p(^3P° \;)3p$	^2D	5/2	$2s2p(^3P° \;)3d$	$^2F°$	7 /2
3	NII	532.0958	2.52e+07	$2s2p^2(^4P)3p$	$^5P°$	1	$2s2p^2(^4P)3d$	^5P	2

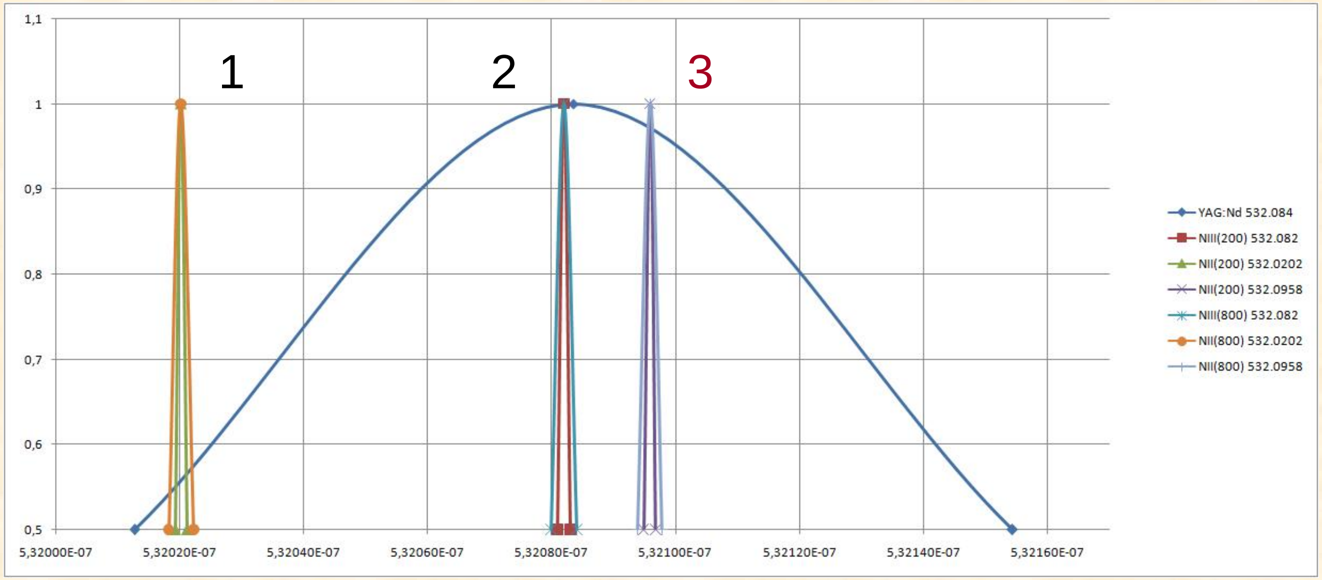

The scattering of laser radiation with a wavelength of 532 nm in the upper atmosphere is caused by excited nitrogen ions.

The density of N^+ exceeds that of N^{++} at altitudes 200–300 km

Diagnostic
of Low Atmosphere and litosphere

- Atmospheric Electrical Field
- Electromagnetic and Acoustic emission of litosphere during deformation changes

Diagnostic allows to study:

The interaction between the upper and low atmospheres

The litosphere effect on ionosphere

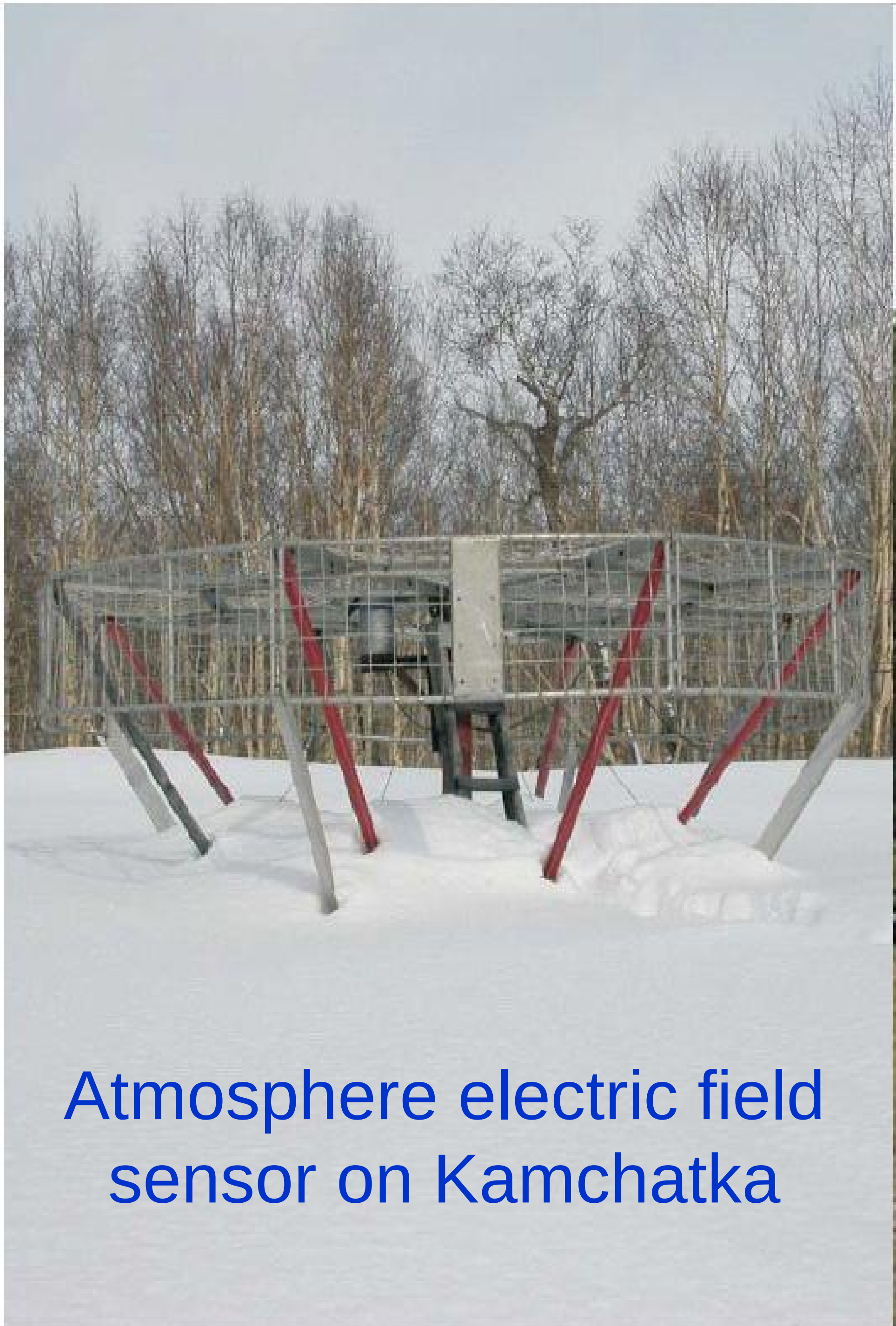

Atmosphere electric field sensor on Kamchatka

Forbush effect in atmospheric electricity

Electro conductivity of air: 1 – positive ions and 2 – negative ions

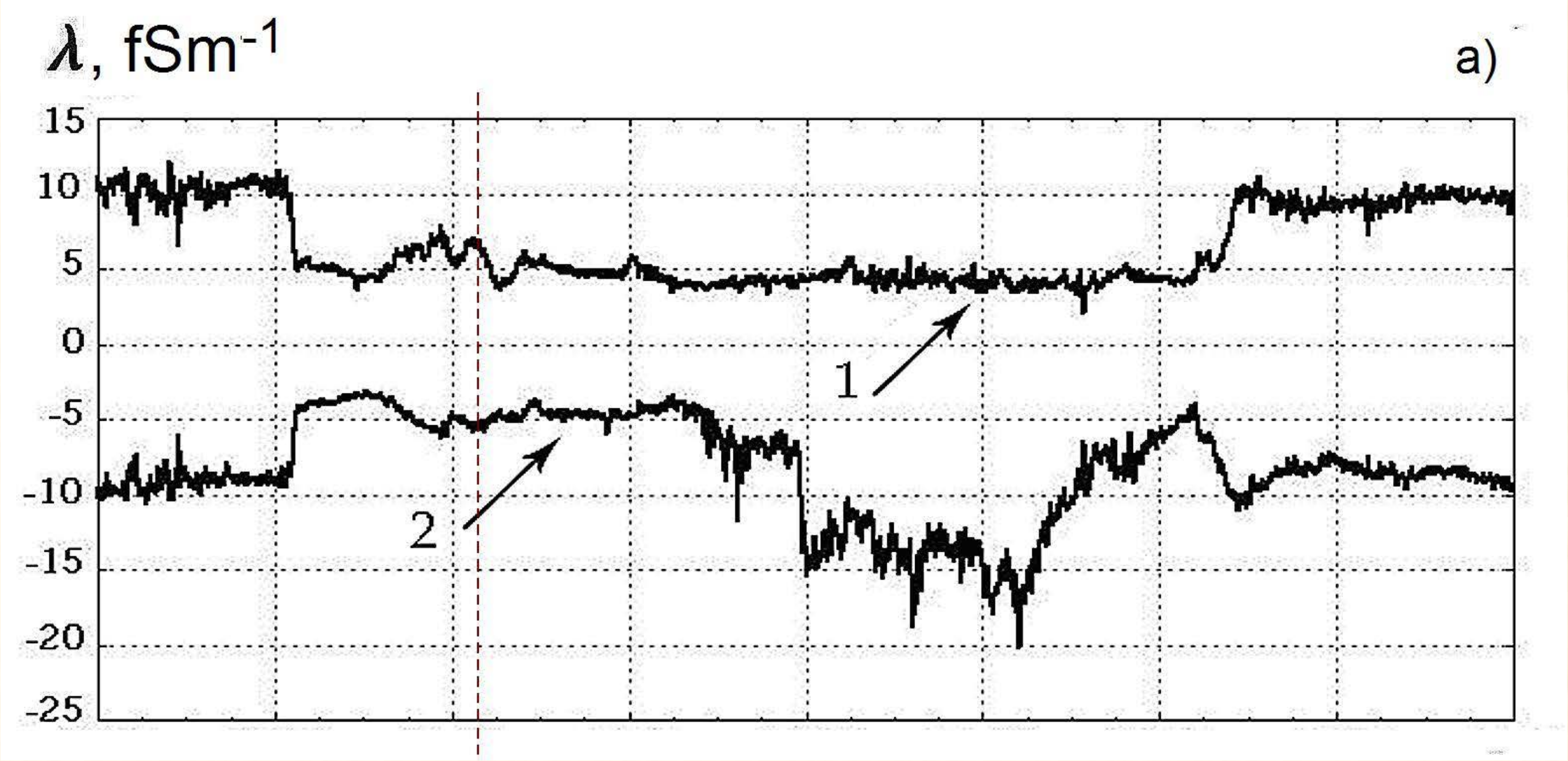

Magnetic and electric processes

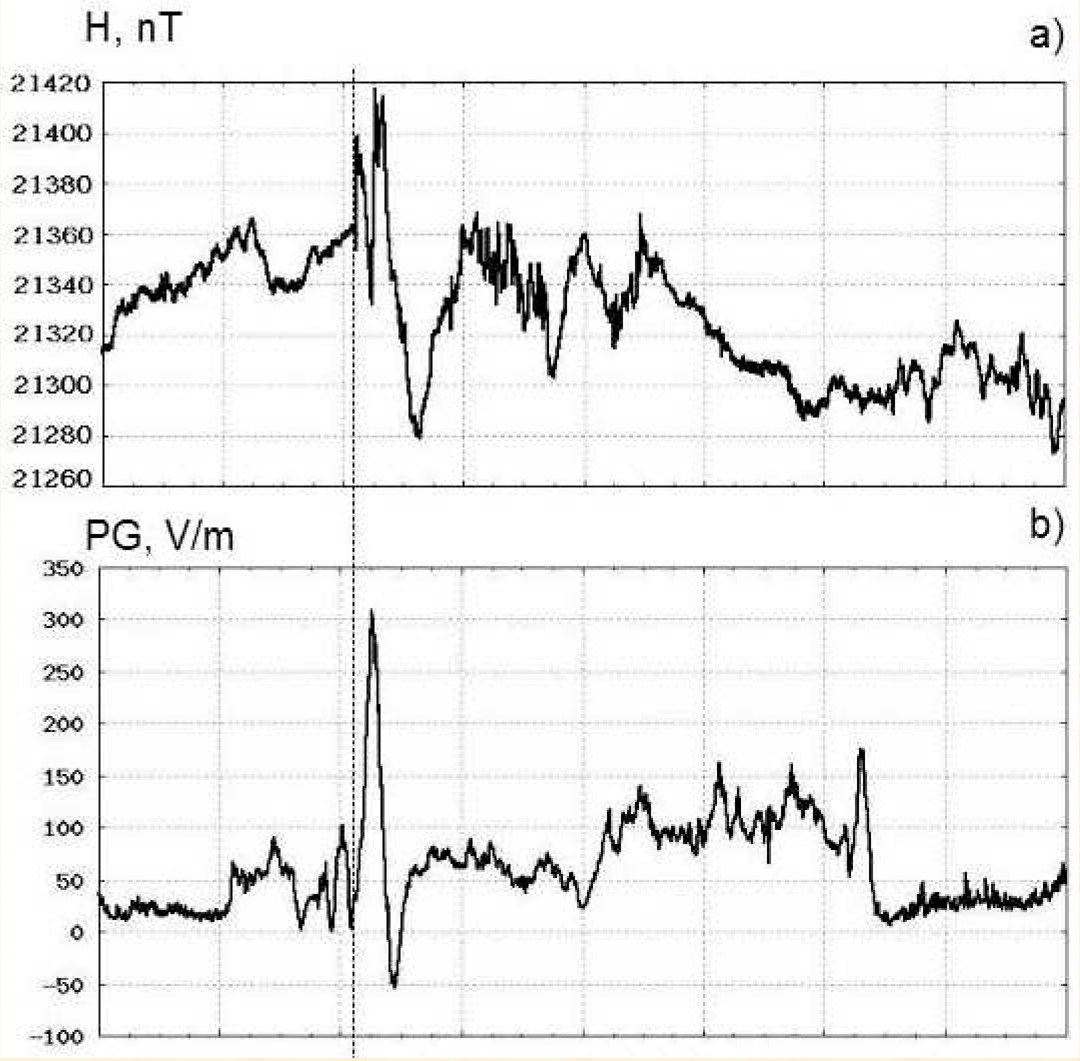

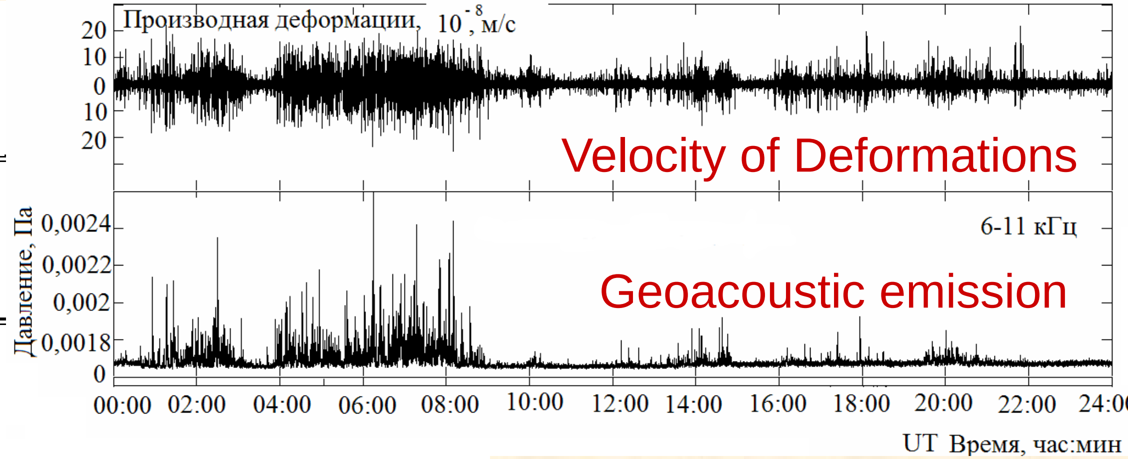

Velocity of Deformations, Geoacoustic emission and Atmosphere electrical field

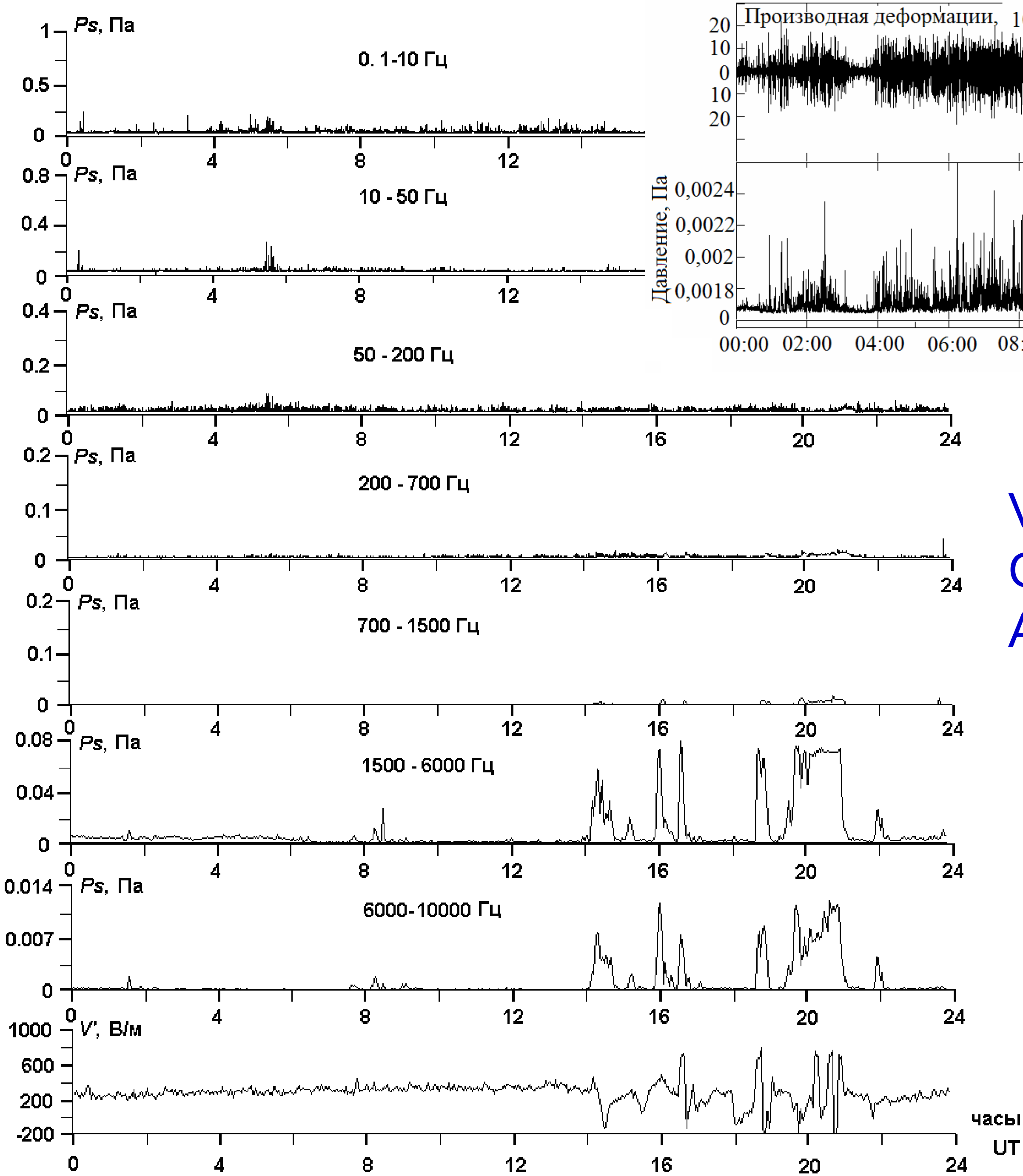

Geoacoustic emission

Atmosphere electrical field

Ionosphere disturbances caused by lithosphere processes

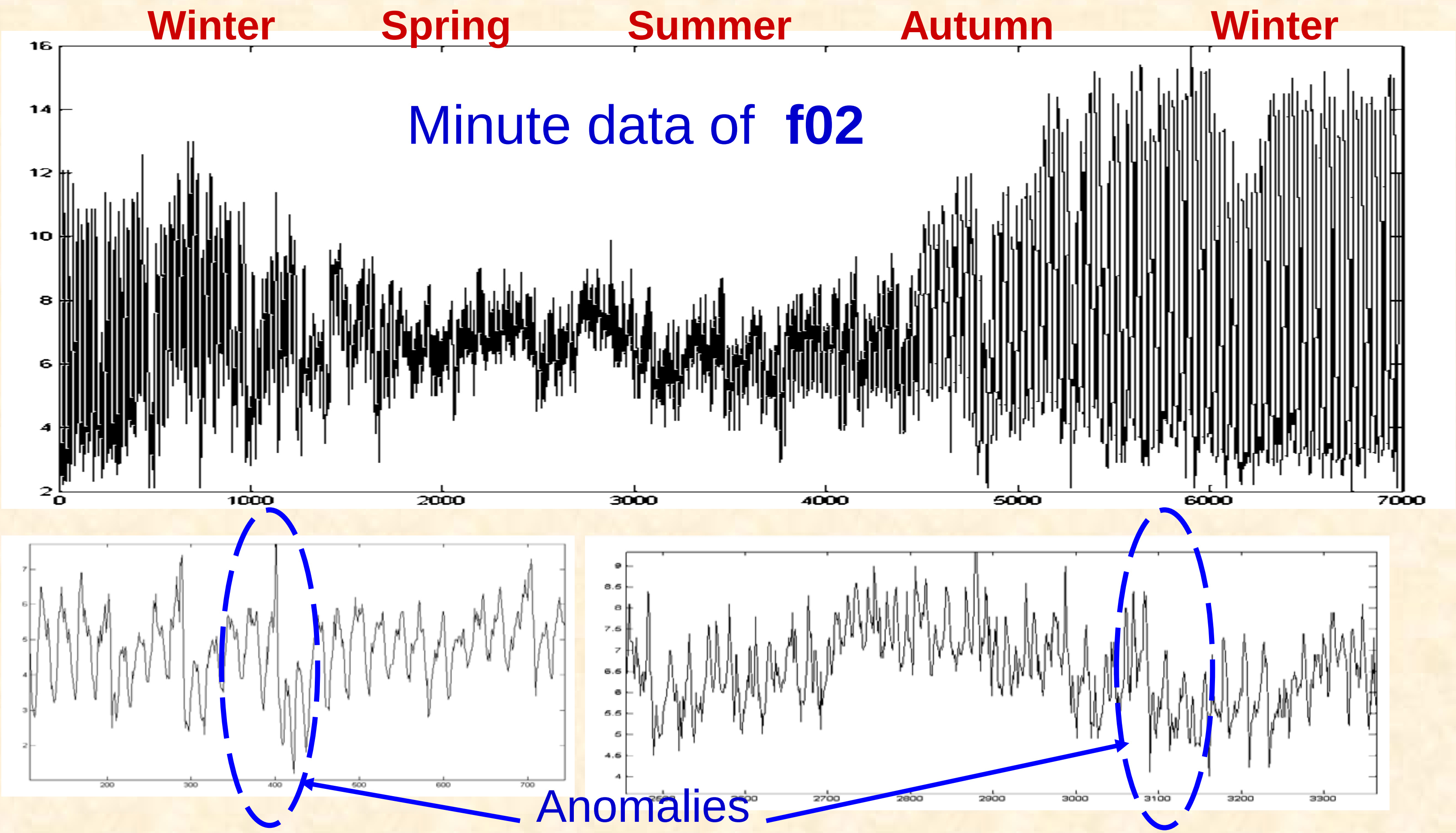

The middle and short period of disturbances

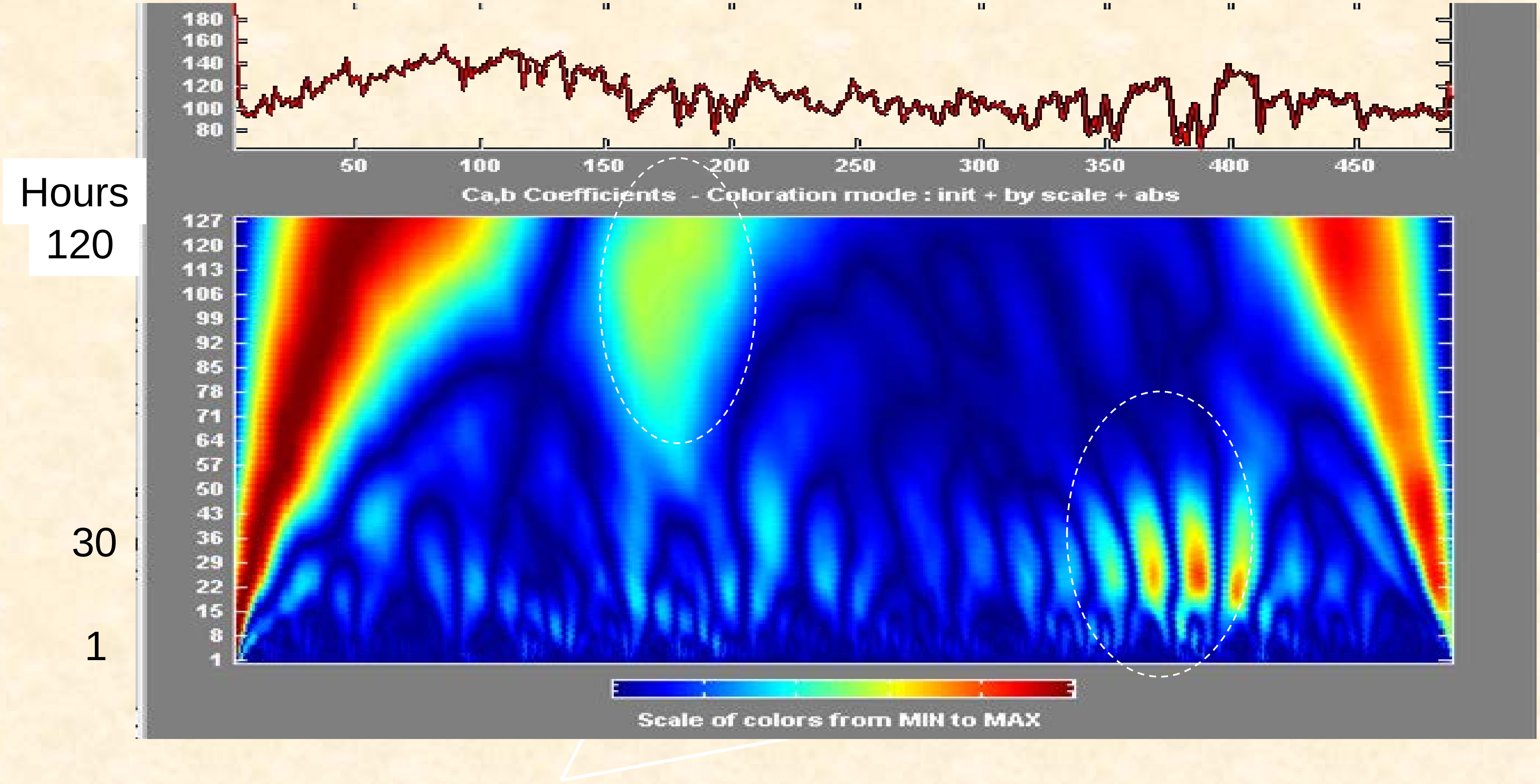

Bogdanov, Mandricova et al.

Conclusion

- The complex Observation System of Space Weather on North Pacific was presented.
- This System was created in collaboration with Japan and European colleges.
- Many years this System is used for investigation of the Space Weather in the Far East region.
- And I can say about a good future of this collaboration!


Station on
Cape Schmidt
Thank for your attention!